Available online at www.sciencedirect.com

ScienceDirect

Nuclear Physics B 921 (2017) 181–210

NUCLEAR PHYSICS B

www.elsevier.com/locate/nuclphysb

CEPC precision of electroweak oblique parameters and weakly interacting dark matter: The fermionic case

Chengfeng Cai [a,1], Zhao-Huan Yu [b,1], Hong-Hao Zhang [a,*]

[a] *School of Physics, Sun Yat-Sen University, Guangzhou 510275, China*
[b] *ARC Centre of Excellence for Particle Physics at the Terascale, School of Physics, The University of Melbourne, Victoria 3010, Australia*

Received 4 February 2017; received in revised form 7 May 2017; accepted 18 May 2017
Available online 25 May 2017
Editor: Hong-Jian He

Abstract

Future electroweak precision measurements in the Circular Electron Positron Collider (CEPC) project would significantly improve the precision of electroweak oblique parameters. We evaluate the expected precision through global fits, and study the corresponding sensitivity to weakly interacting fermionic dark matter. Three models with electroweak multiplets in the dark sector are investigated as illuminating examples. We find that the CEPC data can probe up to TeV scales and explore some regions where direct detection cannot reach, especially when the models respect the custodial symmetry.

1. Introduction

The standard model (SM) has achieved a great success in explaining how the physics happens at subatomic scales. However, there are several puzzles that have not yet been solved. One of the most famous puzzles is dark matter (DM), which makes up most of the matter component in the Universe according to cosmological and astrophysical observations (see, for example, [1–3]

* Corresponding author.
E-mail addresses: caichf@mail2.sysu.edu.cn (C. Cai), zhao-huan.yu@unimelb.edu.au (Z.-H. Yu), zhh98@mail.sysu.edu.cn (H.-H. Zhang).
[1] C. Cai and Z.H. Yu contributed equally to this work.

http://dx.doi.org/10.1016/j.nuclphysb.2017.05.015

for reviews). It is strongly suggested that DM might be some kind of weakly interacting massive particles (WIMPs), as they can give a desired relic abundance through thermal production in the early Universe.

WIMPs are typically introduced in the SM extensions for solving the gauge hierarchy problem, such as supersymmetric [4,5] and extra dimensional [6,7] models. The common ingredient in these models for explaining dark matter is that WIMPs appear as colorless electroweak (EW) multiplets whose electrically neutral components serve as DM candidates. Therefore, it would be more general to consider WIMP models with a dark sector consisting of EW multiplets. The simplest choice is to introduce a multiplet in a nontrivial $\mathrm{SU}(2)_{\mathrm{L}}$ representation and hence the model is called minimal dark matter [8–14]. The next-to-minimal construction is to make use of two $\mathrm{SU}(2)_{\mathrm{L}}$ representations, leading to a wider theoretical landscape and a richer phenomenology [15–29].

The introduction of extra EW multiplets will affect EW precision observables via loop corrections. As a result, accurate measurements of these observables may give some hints to this kind of new physics. Currently, the most precise results come from the measurements in LEP, SLC, Tevatron, and LHC experiments. In particular, the discovery of the Higgs boson [30,31] fixes its mass, the final free parameter in the SM, and hence greatly improves the global electroweak fit [32–35]. The recently proposed circular electron–positron collider (CEPC) in China [36] would mainly serves as a Higgs factory, aiming at precision measurements of the Higgs physics. Besides, it could also carry out new scans around the Z pole and the W^+W^- threshold with a high luminosity, leading to essential improvements for the measurements of most EW precision observables. This would provide an excellent opportunity to indirectly probe WIMP models. Recent works on the CEPC sensitivity to new physics through EW precision measurements include studies on the anomalous hhh and htt couplings through the $e^+e^- \to Zh$ measurement [37–40], natural supersymmetry [41], the anomalous $hZ\gamma$ and $h\gamma\gamma$ couplings through the $e^+e^- \to h\gamma$ measurement [42,43], the anomalous Zbb coupling [44], WIMP models through the $e^+e^- \to f\bar{f}$ measurements [45,46], effective operators [24,47], and so on.

In global fits of EW precision observables, the oblique parameters S, T, and U [48,49] are often introduced to characterize the general effects of new EW particles that do not directly couple to SM fermions. Since a Z_2 symmetry is typically imposed to forbid DM couplings to SM fermions in order to stabilize DM candidates, these parameters are extremely suitable for exploring WIMP models. The CEPC precision of the oblique parameters has been estimated in Ref. [50] and been incorporated into the preliminary conceptual design report of CEPC [36]. However, the results are only obtained under the assumptions of $U = 0$, which is appropriate because U is much smaller than T for a wide class of new physics models. In general, this is not true. For instance, U can be large if there are anomalous triple gauge couplings [51,52]. For this reason, a global fit with free U could be also useful.

In this work, we will at first perform a global fit to derive the CEPC precision of EW oblique parameters, based on the expected uncertainties of EW precision observables in CEPC measurements with the latest updated results. In order to fulfill different needs, we will study the case where S, T, and U are all free parameters, as well as the cases where some of them are fixed to zero. We will then use the fit results to investigate the CEPC capability for testing WIMP models. Only the fermionic DM case will be discussed hereafter. We leave the discussion of the scalar DM case to a future paper.

Renormalizable couplings between fermions and the Higgs must be Yukawa couplings, which require that there are two fermionic multiplets belonging to two $\mathrm{SU}(2)_{\mathrm{L}}$ representations whose dimensions differ by one, because the SM Higgs field is a doublet. We introduce a Z_2 symmetry

to protect DM from decaying. If there is just one vector-like fermionic multiplet in the dark sector, it cannot couple to the Higgs, because it cannot have Yukawa couplings with SM fermions due to the Z_2 symmetry.[2] In this case, the components of the multiplet are degenerate in mass at tree level, because there is no mass contribution from EW symmetry breaking. However, a vector-like fermionic or scalar $SU(2)_L$ multiplet cannot contribute to S, T, or U if its components have exactly degenerate masses [53,54]. Consequently, that kind of fermionic minimal WIMP models (with only one dark sector multiplet) predicts vanishing EW oblique parameters at leading order. Of course, it is *not* the case we plan to discuss in this paper.

The simplest way to avoid it is to consider the kind of fermionic WIMP models with two types of $SU(2)_L$ multiplets whose dimensions differ by one. The two types of fermion multiplets couple to each other by Yukawa interactions with the SM Higgs, and the fermion components will be split when the Higgs field develops a vacuum expectation value (VEV). This kind of models is sensitive to electroweak precision measurements and thus will be detectable at the future high precision electron–positron colliders such as the CEPC. Based on this observation, below we will study three WIMP models with fermionic $SU(2)_L$ multiplets in vector-like representations as illuminating examples:

- Singlet–Doublet Fermionic Dark Matter (SDFDM): one singlet Weyl spinor and two doublet Weyl spinors [15–18,22];
- Doublet–Triplet Fermionic Dark Matter (DTFDM): two doublet Weyl spinors and one triplet Weyl spinor [21];
- Triplet–Quadruplet Fermionic Dark Matter (TQFDM): one triplet Weyl spinor and two quadruplet Weyl spinors [26].

In each model, a Z_2 symmetry is imposed and the dark sector fermionic fields are odd under this symmetry for stabilizing the DM candidate. In order to cancel gauge anomalies, the spinor in the odd-dimensional representation has no hypercharge, while the two spinor in the even-dimensional representation have opposite hypercharges, whose values are assigned to be $\pm 1/2$ for allowing Yukawa couplings with the SM Higgs field. Once the Higgs obtains a non-zero VEV, the neutral components of the multiplets will be mixed up and the lightest mass eigenstate, which is a Majorana fermion, would be a DM candidate.

These models are quite predictive, as there are just four new parameters, two mass parameters and two Yukawa couplings. In addition, they may be treated as subsets of more sophisticated models, sharing some of the related phenomenology. For instance, the SDFDM model may correspond to the bino–Higgsino sector in the MSSM or the singlino–Higgsino sector in the NMSSM, while the DTFDM model may correspond to the Higgsino–wino sector in the MSSM.

The paper is organized as follows. In Section 2, we carry out a global fit to obtain the expected CEPC precision of EW oblique parameters S, T, and U. In Sections 3, 4, and 5, we study the SDFDM, DTFDM, and TQFDM models in details, respectively. We estimate the expected constraints on these models from the oblique parameters with the CEPC precision, as well as current constraints from DM direct detection experiments for comparison. Section 6 gives our conclusions and additional discussions. Appendix A supplements formulas for computing the spin-independent and the spin-dependent DM-nuclei scattering cross sections.

[2] Note that in minimal dark matter models, the Z_2 symmetry is not necessary and the DM is accidentally stable, as long as the multiplet lives in a representation with a sufficient high dimension [8]. But we do not consider such high dimensional representations in this paper.

2. CEPC precision of electroweak oblique parameters

In this section, we perform a global fit to estimate the CEPC precision of EW oblique parameters S, T, and U, based on the expected improvements in future measurements.

2.1. Electroweak oblique parameters

EW radiative corrections can be categorized into two classes, "direct" corrections (vertex, box, and bremsstrahlung corrections) and "oblique" corrections (gauge boson propagator corrections). While the former is process-specific, the latter is not: oblique corrections are universal, as they appear in any process mediated by EW gauge bosons. Oblique corrections can be well organized in the Kennedy–Lynn formalism [55], which uses an effective Lagrangian to incorporate gauge boson vacuum polarization diagrams into a few running couplings. Following this model-independent formalism, Peskin and Takeuchi introduced EW oblique parameters S, T, and U to describe new physics contributions through EW oblique corrections [48,49].

The definitions of these parameters are

$$S = 16\pi[\Pi'_{33}(0) - \Pi'_{3Q}(0)], \tag{2.1}$$

$$T = \frac{4\pi}{s_{\rm W}^2 c_{\rm W}^2 m_{\rm Z}^2}[\Pi_{11}(0) - \Pi_{33}(0)], \tag{2.2}$$

$$U = 16\pi[\Pi'_{11}(0) - \Pi'_{33}(0)], \tag{2.3}$$

where $\Pi'_{IJ}(0) \equiv \partial\Pi_{IJ}(p^2)/\partial p^2|_{p^2=0}$. Π_{11}, Π_{33}, and Π_{3Q} are related to the $g_{\mu\nu}$ coefficients of the vacuum polarization amplitudes of EW gauge bosons contributed by new physics:

$$\Pi_{WW}(p^2) = \frac{e^2}{s_{\rm W}^2}\Pi_{11}(p^2), \tag{2.4}$$

$$\Pi_{ZZ}(p^2) = \frac{e^2}{s_{\rm W}^2 c_{\rm W}^2}[\Pi_{33}(p^2) - 2s_{\rm W}^2\Pi_{3Q}(p^2) + s_{\rm W}^4\Pi_{QQ}(p^2)], \tag{2.5}$$

$$\Pi_{ZA}(p^2) = \frac{e^2}{s_{\rm W}c_{\rm W}}[\Pi_{3Q}(p^2) - s_{\rm W}^2\Pi_{QQ}(p^2)], \tag{2.6}$$

$$\Pi_{AA}(p^2) = e^2\Pi_{QQ}(p^2). \tag{2.7}$$

Here $s_{\rm W} \equiv \sin\theta_{\rm W}$ and $c_{\rm W} \equiv \cos\theta_{\rm W}$ with $\theta_{\rm W}$ denoting the Weinberg angle. S, T, and U are dimensionless by definition. Since only new physics contributions to these parameters are taken into account, SM corresponds to $S = T = U = 0$.

From definitions (2.2) and (2.3) one can easily see that compared with T, U is typically suppressed by a factor of $m_{\rm Z}^2/m_{\rm new}^2$, where $m_{\rm new}$ represents the mass scale of a new EW sector [48]. This point can also be understood in the context of effective field theory as follows. S and T correspond to dimension-6 operators $H^\dagger W^a_{\mu\nu}\sigma^a H B^{\mu\nu}$ and $H^\dagger(D_\mu H)(D^\mu H)^\dagger H$, respectively, while the operator contributing to U in the lowest order is a dimension-8 operator $H^\dagger W^a_{\mu\nu}\sigma^a H H^\dagger W^{b\mu\nu}\sigma^b H$ (see, for instance, Ref. [56] for a review). Thus, many typical new physics models predict $U \ll T$. This is the reason why the assumption $U = 0$ is often adopted in global EW fits. The operator $H^\dagger W^a_{\mu\nu}\sigma^a H B^{\mu\nu}$ means that S is related to the $\mathrm{U(1)_Y}$ gauge field. Actually, the contribution to S from a vector-like fermionic multiplet or a scalar multiplet is proportional to its hypercharge [53,54].

Experimental results show that the observable $\rho = m_W^2/(m_Z^2 c_W^2)$ is extremely close to one [32]. In the SM, $\rho = 1$ is an exact relation at tree level. It has been argued that this relation naturally holds up to EW radiative corrections if the Higgs sector has an $SU(2)_R$ global symmetry. Once the Higgs field obtains a nonzero VEV, the $SU(2)_L \times SU(2)_R$ global symmetry spontaneously breaks down to the unbroken $SU(2)_{L+R}$ symmetry, *i.e.* the so-called custodial symmetry [57]. Under such a symmetry the $SU(2)_L$ gauge bosons W_μ^a $(a = 1, 2, 3)$ transform as a triplet and thus acquire the same mass. This property and the fact that a $U(1)_{em}$ gauge symmetry is unbroken result in $\rho = 1$. In the language of oblique parameters, the deviation of the ρ parameter from one is αT [49,58], and the existence of a custodial symmetry will lead to $T = U = 0$.

In a global EW fit, each EW precision observable O can be split into two parts: $O = O_{SM} + \Delta O(S, T, U)$. The SM contribution O_{SM} should be computed as accurately as possible, and the new physics contribution $\Delta O(S, T, U)$ is a functions of the three oblique parameters. In fact, any $\Delta O(S, T, U)$ should be proportional to one of the following functions [33]:

$$F_1(S, T, U) = S - 2c_W^2 T - \frac{c_W^2 - s_W^2}{2s_W^2} U, \tag{2.8}$$

$$F_2(S, T) = S - 4s_W^2 c_W^2 T, \tag{2.9}$$

$$F_3(S, T) = -10(3 - 8s_W^2)S + (63 - 126s_W^2 - 40s_W^4)T. \tag{2.10}$$

2.2. Electroweak precision observables

In light of the strategy for studying the prospect of EW precision tests used in Refs. [34,50], we adopt a simplified set of precision observables:

1. $\alpha_s(m_Z^2)$, the strong coupling constant at the Z pole;
2. $\Delta\alpha_{had}^{(5)}(m_Z^2)$, the quark sector contribution (without the top quark) to the running of the QED coupling α at the Z pole;
3. m_Z, the Z boson pole mass;
4. m_t, the top quark pole mass;
5. m_h, the Higgs boson pole mass;
6. m_W, the W boson pole mass;
7. $\sin^2\theta_{eff}^{\ell}$, the effective weak mixing angle for the $Z\ell\ell$ coupling;
8. Γ_Z, the Z boson decay width.

In our global fit, the first five observables, as well as S, T, and U, are treated as free parameters. The SM predictions of the remaining three, m_W^{SM}, $(\sin^2\theta_{eff}^{\ell})^{SM}$, and Γ_Z^{SM}, are functions of the free observables, determined by the parametrizations of two-loop radiative corrections in Refs. [59–61]. The new physics contributions are computed with the oblique parameters [33]:

$$\Delta m_W = -\frac{\alpha m_W^{SM}}{4(c_W^2 - s_W^2)} F_1(S, T, U), \tag{2.11}$$

$$\Delta\sin^2\theta_{eff}^{\ell} = \frac{\alpha}{4(c_W^2 - s_W^2)} F_2(S, T), \tag{2.12}$$

$$\Delta\Gamma_Z = \frac{\alpha^2 m_Z}{72 s_W^2 c_W^2 (c_W^2 - s_W^2)} F_3(S, T). \tag{2.13}$$

Table 1
Current measurement values and CEPC baseline (CEPC-B) precisions of EW precision observables. The subscripts "ex" and "th" denote experimental and theoretical uncertainties, respectively. For the unspecified uncertainties, theoretical uncertainties are either neglected or incorporated.

	Current data	CEPC-B precision
$\alpha_s(m_Z^2)$	0.1185 ± 0.0006 [32]	$\pm 1 \times 10^{-4}$ [62]
$\Delta\alpha^{(5)}_{\rm had}(m_Z^2)$	0.02765 ± 0.00008 [63]	$\pm 4.7 \times 10^{-5}$ [34,64]
m_Z [GeV]	91.1875 ± 0.0021 [65]	$\pm 5 \times 10^{-4}$ [36]
m_t [GeV]	$173.34 \pm 0.76_{\rm ex}$ [66] $\pm 0.5_{\rm th}$ [67]	$\pm 0.2_{\rm ex}$ [68] $\pm 0.5_{\rm th}$ [67]
m_h [GeV]	125.09 ± 0.24 [69]	$\pm 5.9 \times 10^{-3}$ [36]
m_W [GeV]	$80.385 \pm 0.015_{\rm ex}$ [32] $\pm 0.004_{\rm th}$ [59]	$(\pm 3_{\rm ex}$ [36] $\pm 1_{\rm th}$ [70]$) \times 10^{-3}$
$\sin^2\theta^\ell_{\rm eff}$	0.23153 ± 0.00016 [65]	$(\pm 2.3_{\rm ex}$ [36] $\pm 1.5_{\rm th}$ [70]$) \times 10^{-5}$
Γ_Z [GeV]	2.4952 ± 0.0023 [65]	$(\pm 5_{\rm ex}$ [36] $\pm 0.8_{\rm th}$ [50,71]$) \times 10^{-4}$

Table 2
CEPC improved (CEPC-I) precisions of m_Z, Γ_Z, and m_t taking into account their potential improvements.

	CEPC-I precision
m_Z [GeV]	$\pm 1 \times 10^{-4}$ [36]
Γ_Z [GeV]	$(\pm 1_{\rm ex}$ [36] $\pm 0.8_{\rm th}$ [50,71]$) \times 10^{-4}$
m_t [GeV]	$\pm 0.03_{\rm ex} \pm 0.1_{\rm th}$ [72]

Table 1 shows the current measurement values and CEPC baseline precisions (denoted as "CEPC-B" hereafter) of the eight EW precision observables. The references for these values are also listed in the table. Experimental ("ex") and theoretical ("th") uncertainties are separately denoted for some values. For those unspecified uncertainties, theoretical uncertainties are either neglected or incorporated into the total uncertainties.

Experimental uncertainties for the CEPC-B precisions will be mostly reduced by the running of CEPC, according to the preliminary conceptual design report of CEPC [36]. Exceptions are the potential reduction of the $\alpha_s(m_Z^2)$ uncertainty due to lattice QCD calculation in the next decade [62], the improvement of the $\Delta\alpha^{(5)}_{\rm had}(m_Z^2)$ measurement from ongoing charm and bottom factories as well as lattice QCD prediction [34], and the improvement of the m_t measurement at the high-luminosity LHC [68]. We also consider that the theoretical uncertainties of m_W, $\sin^2\theta^\ell_{\rm eff}$, and Γ_Z can be reduced by fully calculating three-loop corrections in the future [50,70,71].

There may be some further improvements. A high-precision calibration of the beam energy may be achieved at the CEPC, reducing the experimental uncertainties of m_Z and Γ_Z down to 0.1 MeV [36]. The current CEPC plan does not include a $t\bar{t}$ threshold scan. Nevertheless, if the ILC would preform this kind of scan before or during the running of CEPC, the experimental and theoretical uncertainties of m_t could be reduced to 30 and 100 MeV, respectively [72]. These potential improvements are collected in Table 2, and the corresponding precisions are denoted as "CEPC-I" hereafter.

2.3. Global fits

We calculate a modified χ^2 function for global fits [50]:

Table 3
Fit results for S, T, and U with current, CEPC-B, and CEPC-I precisions. σ_i and ρ_{ij} $(i, j = S, T, U)$ are the standard deviations and the correlation coefficients, respectively.

	σ_S	σ_T	σ_U	ρ_{ST}	ρ_{SU}	ρ_{TU}
Current	0.10	0.12	0.094	+0.89	−0.55	−0.80
CEPC-B	0.021	0.026	0.020	+0.90	−0.68	−0.84
CEPC-I	0.011	0.0071	0.010	+0.74	+0.15	−0.21

$$\chi^2_{\rm mod} = \sum_i \left(\frac{O_i^{\rm meas} - O_i^{\rm pred}}{\sigma_i} \right)^2 + \sum_j \left\{ -2 \ln \left[{\rm erf} \left(\frac{O_j^{\rm meas} - O_j^{\rm pred} + \delta_j}{\sqrt{2}\sigma_j} \right) - {\rm erf} \left(\frac{O_j^{\rm meas} - O_j^{\rm pred} - \delta_j}{\sqrt{2}\sigma_j} \right) \right] \right\}, \tag{2.14}$$

where $O_i^{\rm meas}$ and $O_i^{\rm pred}$ denote the measured and predicted values of the observables. For the free observables, we take the mean values of the current measurements as $O_i^{\rm meas}$. Meanwhile, $O_i^{\rm meas}$ for the induced observables m_W, $\sin^2\theta^\ell_{\rm eff}$, and Γ_Z are set to be their SM prediction values. By this way, the mean values of the oblique parameters in the fit result will locate at zero, and thus the current and CEPC precisions are just represented by the uncertainties of S, T, and U, which will be expressed by standard deviations and correlation coefficients. The first term in Eq. (2.14) is an ordinary χ^2, corresponding to the observables whose uncertainties σ_i are not split into two parts in Tables 1 and 2. The other observables belong to the second term, which treats the experimental uncertainties σ_j as Gaussian errors while the theoretical uncertainties δ_j as flat box-shaped errors, following Refs. [50,73–75].

We utilize the code `MultiNest` [76] to perform a quick and stable global fit. Firstly, we treat all of S, T, and U as free parameters, and obtain the fit results presented in Table 3. Fig. 1 demonstrates the corresponding 95% CL contours in the $S-T$, $S-U$, and $T-U$ planes. We can see that the running of CEPC will greatly improve the precision of the oblique parameters. Correlation relations among these parameters are not quite definite: the sign of ρ_{SU} in the CEPC-I precisions is different from those in the current and CEPC-B precisions. Nonetheless, the correlation between S and T seems positive and close to one. This can be easily understood from Eqs. (2.8)–(2.9), whose numerical results are

$$F_1 = S - 1.55T - 1.24U, \quad F_2 = S - 0.69T, \quad F_3 = -12.2(S - 2.7T). \tag{2.15}$$

Therefore, the increase of S can be always compensated by increasing T, leading to a high positive correlation [32,77].

Moreover, we carry out the global fit with some of the oblique parameters fixed to zero. We separately consider two assumptions by fixing one parameter to zero: (a) the assumption of $U = 0$, which is useful for new physics models predicting a tiny U; (b) the assumption of $S = 0$, which often holds for introducing new $\mathrm{SU(2)_L}$ multiplets with zero hypercharge. The fit results are listed in Table 4 and the corresponding contours in the $S-T$ or $T-U$ plane at 95% CL are shown in Fig. 2. For the $U = 0$ case, S and T always have a high positive correlation as expected. The result is consistent with those given in Refs. [36,50]. For the $S = 0$ case, the F_1 function in Eq. (2.15) results in a negative correlation between T and U.

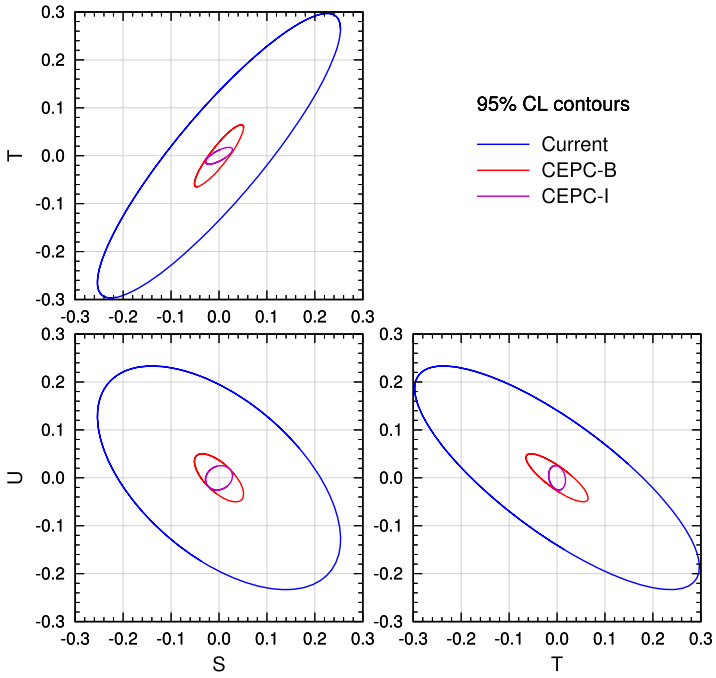

Fig. 1. 95% CL contours in the $S-T$, $S-U$, and $T-U$ planes for current, CEPC-B, and CEPC-I precisions.

Table 4
Fit results with current, CEPC-B, and CEPC-I precisions under the assumptions of $U=0$ (a) and $S=0$ (b). σ_i and ρ_{ij} $(i,j=S,T,U)$ are the standard deviations and the correlation coefficients, respectively.

(a) $U=0$ fixed

	σ_S	σ_T	ρ_{ST}
Current	0.085	0.072	+0.90
CEPC-B	0.015	0.014	+0.83
CEPC-I	0.011	0.0069	+0.80

(b) $S=0$ fixed

	σ_T	σ_U	ρ_{TU}
Current	0.054	0.078	−0.81
CEPC-B	0.011	0.015	−0.72
CEPC-I	0.0048	0.010	−0.48

We also present fit results for fixing two oblique parameters to zero. In Table 5(a), the results for the S parameter are obtained under the assumption of $T=U=0$, which corresponds to the models that respect a custodial symmetry. In Table 5(b), we give the results for the T parameter under the assumption of $S=U=0$. They are useful for the models that contain new $\mathrm{SU(2)_L}$ multiplets with zero hypercharge and also predict $U \ll T$.

Below, we use the above results to estimate the expected constraints on the fermionic WIMP models.

3. Singlet–doublet fermionic dark matter

3.1. Fields and interactions

In the SDFDM model, we introduce three left-handed Weyl spinors [15–18,22]:

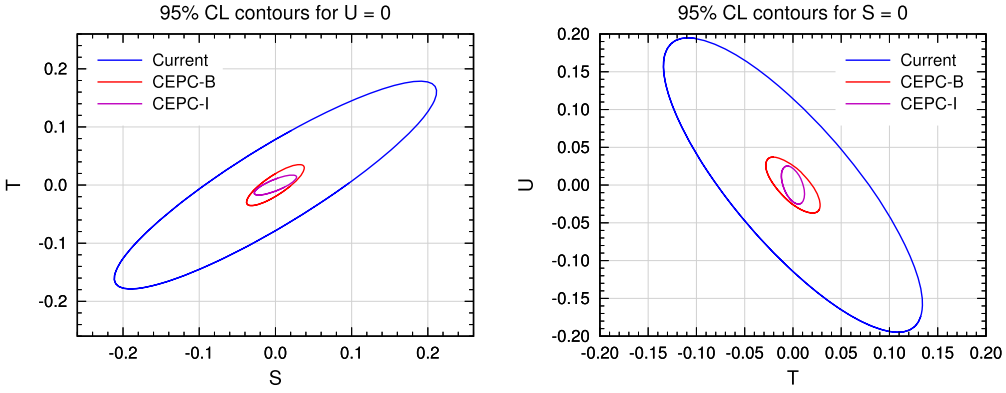

(a) $U = 0$ fixed (b) $S = 0$ fixed

Fig. 2. 95% CL contours in the $S - T$ (a) and $T - U$ (b) plane for current, CEPC-B, and CEPC-I precisions under the assumptions of $U = 0$ (a) and $S = 0$ (b).

Table 5
Fit results with current, CEPC-B, and CEPC-I precisions under the assumptions of $T = U = 0$ (a) and $S = U = 0$ (b). σ_S and σ_T are the standard deviations of S and T, respectively.

(a) $T = U = 0$ fixed

	σ_S
Current	0.037
CEPC-B	0.0085
CEPC-I	0.0068

(b) $S = U = 0$ fixed

	σ_T
Current	0.032
CEPC-B	0.0079
CEPC-I	0.0042

$$S \in (\mathbf{1}, 0), \quad D_1 = \begin{pmatrix} D_1^0 \\ D_1^- \end{pmatrix} \in (\mathbf{2}, -1/2), \quad D_2 = \begin{pmatrix} D_2^+ \\ D_2^0 \end{pmatrix} \in (\mathbf{2}, +1/2). \tag{3.1}$$

Their gauge transformations under $(\mathrm{SU}(2)_\mathrm{L}, \mathrm{U}(1)_\mathrm{Y})$ are denoted. The kinetic and interacting properties are encoded in the following Lagrangians:

$$\mathcal{L}_\mathrm{S} = i S^\dagger \bar{\sigma}^\mu \partial_\mu S - \frac{1}{2}(m_S S S + \mathrm{h.c.}), \tag{3.2}$$

$$\mathcal{L}_\mathrm{D} = i D_1^\dagger \bar{\sigma}^\mu D_\mu D_1 + i D_2^\dagger \bar{\sigma}^\mu D_\mu D_2 - (m_D \epsilon_{ij} D_1^i D_2^j + \mathrm{h.c.}), \tag{3.3}$$

$$\mathcal{L}_\mathrm{HSD} = y_1 H_i S D_1^i - y_2 H_i^\dagger S D_2^i + \mathrm{h.c.}, \tag{3.4}$$

where H is the SM Higgs doublet and D_μ is the covariant derivative. Gauge interactions of the doublets are

$$\begin{aligned} \mathcal{L}_\mathrm{D} \supset\ & \frac{g}{\sqrt{2}}[W_\mu^+ (D_1^0)^\dagger \bar{\sigma}^\mu D_1^- + W_\mu^- (D_1^-)^\dagger \bar{\sigma}^\mu D_1^0 + W_\mu^+ (D_2^+)^\dagger \bar{\sigma}^\mu D_2^0 + W_\mu^- (D_2^0)^\dagger \bar{\sigma}^\mu D_2^+] \\ & + \frac{g}{2c_\mathrm{W}} Z_\mu (D_1^0)^\dagger \bar{\sigma}^\mu D_1^0 + \left[-eA_\mu + \frac{g}{2c_\mathrm{W}}(s_\mathrm{W}^2 - c_\mathrm{W}^2) Z_\mu \right] (D_1^-)^\dagger \bar{\sigma}^\mu D_1^- \\ & - \frac{g}{2c_\mathrm{W}} Z_\mu (D_2^0)^\dagger \bar{\sigma}^\mu D_2^0 + \left[eA_\mu - \frac{g}{2c_\mathrm{W}}(s_\mathrm{W}^2 - c_\mathrm{W}^2) Z_\mu \right] (D_2^+)^\dagger \bar{\sigma}^\mu D_2^+. \end{aligned} \tag{3.5}$$

In the unitary gauge, $H = (0, (v+h)/\sqrt{2})^{\mathrm{T}}$ with the VEV $v \approx 246$ GeV, and the mass terms are

$$\begin{aligned}\mathcal{L}_{\mathrm{mass}} &= -\frac{1}{2}(S \quad D_1^0 \quad D_2^0)\mathcal{M}_{\mathrm{N}}\begin{pmatrix} S \\ D_1^0 \\ D_2^0 \end{pmatrix} - m_D D_1^- D_2^+ + \mathrm{h.c.} \\ &= -\frac{1}{2}\sum_{i=1}^{3} m_{\chi_i^0}\chi_i^0\chi_i^0 - m_{\chi^\pm}\chi^-\chi^+ + \mathrm{h.c.}\,, \end{aligned} \tag{3.6}$$

where we define the mass matrix and the fields as

$$\mathcal{M}_{\mathrm{N}} = \begin{pmatrix} m_S & \frac{1}{\sqrt{2}}y_1 v & \frac{1}{\sqrt{2}}y_2 v \\ \frac{1}{\sqrt{2}}y_1 v & 0 & -m_D \\ \frac{1}{\sqrt{2}}y_2 v & -m_D & 0 \end{pmatrix}, \quad m_{\chi^\pm} = m_D, \quad \chi^+ = D_2^+, \quad \chi^- = D_1^-, \tag{3.7}$$

$$\mathcal{N}^{\mathrm{T}}\mathcal{M}_{\mathrm{N}}\mathcal{N} = \mathrm{diag}(m_{\chi_1^0}, m_{\chi_2^0}, m_{\chi_3^0}), \quad \begin{pmatrix} S \\ D_1^0 \\ D_2^0 \end{pmatrix} = \mathcal{N}\begin{pmatrix} \chi_1^0 \\ \chi_2^0 \\ \chi_3^0 \end{pmatrix}. \tag{3.8}$$

Thus, the new mass states are one singly charged fermion $\chi^\pm$ and three Majorana fermions $\chi_{1,2,3}^0$, where the lightest neutral fermion χ_1^0 serves as a DM candidate.

The Lagrangian for the trilinear interaction between χ_1^0 and the Higgs boson is

$$\mathcal{L}_{h\chi_1^0\chi_1^0} = \frac{1}{2}g_{h\chi_1^0\chi_1^0}h\bar{\chi}_1^0\chi_1^0, \tag{3.9}$$

where the $h\chi_1^0\chi_1^0$ coupling is given by

$$g_{h\chi_1^0\chi_1^0} = -\sqrt{2}(y_1\mathcal{N}_{21} + y_2\mathcal{N}_{31})\mathcal{N}_{11}. \tag{3.10}$$

This coupling induces spin-independent (SI) DM-nucleus scattering. Since χ_1^0 is a Majorana fermion, the vector current operator $\bar{\chi}_1^0\gamma^\mu\chi_1^0$ vanishes. Thus, χ_1^0 can only couple to Z through an axial current interaction Lagrangian

$$\mathcal{L}_{Z\chi_1^0\chi_1^0} = \frac{1}{2}g_{Z\chi_1^0\chi_1^0}Z_\mu\bar{\chi}_1^0\gamma^\mu\gamma_5\chi_1^0, \tag{3.11}$$

where the $Z\chi_1^0\chi_1^0$ coupling is

$$g_{Z\chi_1^0\chi_1^0} = -\frac{g}{2c_{\mathrm{W}}}(|\mathcal{N}_{21}|^2 - |\mathcal{N}_{31}|^2). \tag{3.12}$$

This coupling will not induce SI scattering, but it leads to spin-dependent (SD) scattering. Direct detection experiments search for recoil signals from DM-nucleus scattering and could be sensitive to χ_1^0. Related formulas are collected in Appendix A.

3.2. Vacuum polarizations and custodial symmetry

The dark sector fermions affect the vacuum polarizations of EW gauge bosons at one-loop level, and hence contribute to the EW oblique parameters S, T, and U. Their contributions to the vacuum polarizations are given by

$$\Pi_{AA}(p^2) = \frac{2e^2}{16\pi^2} J_2(p^2, m^2_{\chi^\pm}), \qquad \Pi_{ZA}(p^2) = \frac{2e g_{Z\chi^+\chi^-}}{16\pi^2} J_2(p^2, m^2_{\chi^\pm}), \tag{3.13}$$

$$\begin{aligned}\Pi_{ZZ}(p^2) = \frac{1}{16\pi^2}\Bigg\{ &\sum_{i,j=1}^{3} \Big[|g_{Z\chi^0_i\chi^0_j}|^2 J_1(p^2, m^2_{\chi^0_i}, m^2_{\chi^0_j}) \\ &+ m_{\chi^0_i} m_{\chi^0_j} (g^2_{Z\chi^0_i\chi^0_j} + \text{h.c.}) B_0(p^2, m^2_{\chi^0_i}, m^2_{\chi^0_j})\Big] \\ &+ 2g^2_{Z\chi^+\chi^-}\Big[J_1(p^2, m^2_{\chi^\pm}, m^2_{\chi^\pm}) - 2m^2_{\chi^\pm} B_0(p^2, m^2_{\chi^\pm}, m^2_{\chi^\pm})\Big]\Bigg\},\end{aligned} \tag{3.14}$$

$$\begin{aligned}\Pi_{WW}(p^2) = \frac{1}{16\pi^2}\sum_{j=1}^{3}\Big[&(|a_{W\chi^+\chi^0_j}|^2 + |b_{W\chi^+\chi^0_j}|^2) J_1(p^2, m^2_{\chi^0_j}, m^2_{\chi^\pm}) \\ &- 2m_{\chi^0_j} m_{\chi^\pm} (a_{W\chi^+\chi^0_j} b^*_{W\chi^+\chi^0_j} + \text{h.c.}) B_0(p^2, m^2_{\chi^0_j}, m^2_{\chi^\pm})\Big].\end{aligned} \tag{3.15}$$

We define couplings

$$g_{Z\chi^+\chi^-} = \frac{g(c^2_{\rm W} - s^2_{\rm W})}{2c_{\rm W}}, \quad g_{Z\chi^0_i\chi^0_j} = -\frac{g}{2c_{\rm W}}(\mathcal{N}_{2,i}\mathcal{N}^*_{2,j} - \mathcal{N}_{3,i}\mathcal{N}^*_{3,j}), \tag{3.16}$$

$$a_{W\chi^+\chi^0_j} = \frac{g}{\sqrt{2}}\mathcal{N}_{3,j}, \quad b_{W\chi^+\chi^0_j} = -\frac{g}{\sqrt{2}}\mathcal{N}^*_{2,j}, \tag{3.17}$$

and functions

$$\begin{aligned}J_1(p^2, m_1^2, m_2^2) &= A_0(m_1^2) + A_0(m_2^2) - (p^2 - m_1^2 - m_2^2) B_0(p^2, m_1^2, m_2^2) \\ &\quad - 4B_{00}(p^2, m_1^2, m_2^2),\end{aligned} \tag{3.18}$$

$$\begin{aligned}J_2(p^2, m^2) &= J_1(p^2, m^2, m^2) - 2m^2 B_0(p^2, m^2, m^2) \\ &= 2A_0(m^2) - p^2 B_0(p^2, m^2, m^2) - 4B_{00}(p^2, m^2, m^2),\end{aligned} \tag{3.19}$$

where the Passiano–Veltman scalar functions [78] have consistent definitions with Ref. [79]:

$$A_0(m^2) = \frac{(2\pi Q)^{4-d}}{i\pi^2}\int d^d q \frac{1}{q^2 - m^2 + i\varepsilon}, \tag{3.20}$$

$$B_0(p^2, m_1^2, m_2^2) = \frac{(2\pi Q)^{4-d}}{i\pi^2}\int d^d q \frac{1}{[q^2 - m_1^2 + i\varepsilon][(q+p)^2 - m_2^2 + i\varepsilon]}, \tag{3.21}$$

$$\begin{aligned}&g_{\mu\nu} B_{00}(p^2, m_1^2, m_2^2) + p_\mu p_\nu B_{11}(p^2, m_1^2, m_2^2) \\ &= \frac{(2\pi Q)^{4-d}}{i\pi^2}\int d^d q \frac{q_\mu q_\nu}{[q^2 - m_1^2 + i\varepsilon][(q+p)^2 - m_2^2 + i\varepsilon]}.\end{aligned} \tag{3.22}$$

We use `LoopTools` [80] to give numerical values for these functions.

For $m_1 = m_2 = m$, we have

$$J_1'(0,m^2,m^2) = -\frac{2}{3}\Delta + \frac{2}{3}\ln\frac{m^2}{Q^2} + \frac{1}{3}, \tag{3.23}$$

$$B_0'(0,m^2,m^2) = \frac{1}{6m^2}, \tag{3.24}$$

where $\Delta \equiv 2/(4-d) - \gamma_{\rm E} + \ln 4\pi$ is the UV-divergent term. If $m_1 \ll m_2$, the following approximations hold:

$$J_1'(0,m_1^2,m_2^2) \approx -\frac{2}{3}\Delta + \frac{2}{3}\ln\frac{m_2^2}{Q^2} - \frac{2}{9} + \mathcal{O}\left(\frac{m_1^2}{m_2^2}\right), \tag{3.25}$$

$$B_0'(0,m_1^2,m_2^2) \approx \frac{1}{2m_2^2} + \mathcal{O}\left(\frac{m_1^2}{m_2^4}\right). \tag{3.26}$$

These expressions are useful for the analyses below.

When $y_1 = y_2 = y$, there is a custodial global symmetry in this model. It can be clarified by defining $\mathrm{SU}(2)_{\rm R}$ doublets

$$(\mathcal{D}^A)^i = \begin{pmatrix} D_1^i \\ D_2^i \end{pmatrix}, \quad (\mathcal{H}^A)_i = \begin{pmatrix} H_i^\dagger \\ H_i \end{pmatrix}, \tag{3.27}$$

since the Lagrangians has $\mathrm{SU}(2)_{\rm L} \times \mathrm{SU}(2)_{\rm R}$ invariant forms

$$\mathcal{L}_{\rm D} = i\mathcal{D}_A^\dagger \bar{\sigma}^\mu D_\mu \mathcal{D}^A - \frac{1}{2}[m_D \epsilon_{AB}\epsilon_{ij}(\mathcal{D}^A)^i(\mathcal{D}^B)^j + \text{h.c.}], \tag{3.28}$$

$$\mathcal{L}_{\rm HSD} = y(H_i S D_1^i - H_i^\dagger S D_2^i) + \text{h.c.} = y\epsilon_{AB}(\mathcal{H}^A)_i S(\mathcal{D}^B)^j + \text{h.c.} \tag{3.29}$$

Therefore, it is expected to have vanishing T and U in this custodial symmetry limit.

Moreover, there are other important implications in this limit: at tree level, the SD DM-nucleon scattering cross section vanishes, and the SI scattering cross section vanishes as well if $m_S > m_D$. The first implication can be easily understood. The custodial symmetry ensures the up and down components of the $\mathrm{SU}(2)_{\rm R}$ doublet $\mathcal{D}_A$ have equal Dirac mass terms induced by the nonzero VEV. Consequently, each neutral mass state χ_i^0 has equal D_1 and D_2 components ($|\mathcal{N}_{21}| = |\mathcal{N}_{31}|$). Since D_1 and D_2 have opposite hypercharges and opposite third components of weak isospin, the $Z\chi_i^0\chi_i^0$ couplings becomes zero due to the exact cancellation, leading to a vanishing SD scattering cross section. The second implication is not as obvious as the first one, but we can understand both through the following analysis.

In the $y_1 = y_2 = y$ limit, if $m_S > m_D$, the mass matrix $\mathcal{M}_{\rm N}$ can be diagonalized by the mixing matrix

$$\mathcal{N} = \begin{pmatrix} 0 & is_\beta & c_\beta \\ \frac{1}{\sqrt{2}} & -\frac{ic_\beta}{\sqrt{2}} & \frac{s_\beta}{\sqrt{2}} \\ -\frac{1}{\sqrt{2}} & -\frac{ic_\beta}{\sqrt{2}} & \frac{s_\beta}{\sqrt{2}} \end{pmatrix}, \tag{3.30}$$

where s_β and c_β are some real numbers satisfying $s_\beta^2 + c_\beta^2 = 1$. The mass eigenvalues are

$$m_{\chi_1^0} = m_D, \tag{3.31}$$

$$m_{\chi_2^0} = \frac{1}{2}[\sqrt{(m_D + m_S)^2 + 4y^2v^2} - m_S + m_D], \tag{3.32}$$

$$m_{\chi_3^0} = \frac{1}{2}[\sqrt{(m_D + m_S)^2 + 4y^2v^2} + m_S - m_D]. \tag{3.33}$$

Substituting $\mathcal{N}_{11} = 0$ and $\mathcal{N}_{21} = -\mathcal{N}_{31} = 1/\sqrt{2}$ into Eqs. (3.10) and (3.12), one finds $g_{Z\chi_1^0\chi_1^0} = g_{h\chi_1^0\chi_1^0} = 0$. Therefore, direct detection experiments can hardly constrain the model in this case.

If $m_S < m_D$, the mass eigenvalues become

$$m_{\chi_1^0} = \min\left(m_D,\ \frac{1}{2}[\sqrt{(m_D + m_S)^2 + 4y^2v^2} + m_S - m_D]\right), \tag{3.34}$$

$$m_{\chi_2^0} = \max\left(m_D,\ \frac{1}{2}[\sqrt{(m_D + m_S)^2 + 4y^2v^2} + m_S - m_D]\right), \tag{3.35}$$

$$m_{\chi_3^0} = \frac{1}{2}[\sqrt{(m_D + m_S)^2 + 4y^2v^2} - m_S + m_D]. \tag{3.36}$$

There are two kinds of mass order. If $m_{\chi_1^0} = m_D$, the $\mathcal{N}$ matrix remains the form of Eq. (3.30), leading to $g_{Z\chi_1^0\chi_1^0} = g_{h\chi_1^0\chi_1^0} = 0$. Otherwise we should multiply (3.30) by a permutation matrix to obtain the correct mass order:

$$\mathcal{N} \to \mathcal{N}\begin{pmatrix} 0 & 1 & 0 \\ 1 & 0 & 0 \\ 0 & 0 & 1 \end{pmatrix} = \begin{pmatrix} is_\beta & 0 & c_\beta \\ -\frac{ic_\beta}{\sqrt{2}} & \frac{1}{\sqrt{2}} & \frac{s_\beta}{\sqrt{2}} \\ -\frac{ic_\beta}{\sqrt{2}} & -\frac{1}{\sqrt{2}} & \frac{s_\beta}{\sqrt{2}} \end{pmatrix}. \tag{3.37}$$

This still leads to a vanishing $g_{Z\chi_1^0\chi_1^0}$, but $g_{h\chi_1^0\chi_1^0}$ becomes nonzero. Thus, there will be some constraints from SI direct detection.

Furthermore, $y_1 = -y_2$ corresponds to another custodial symmetry limit, which can easily examined by instead defining $(\mathcal{H}^A)_i = (-H_i^\dagger, H_i)$. In this limit, we also have $T = U = 0$ and $g_{Z\chi_1^0\chi_1^0} = 0$.

3.3. Expected constraints

Fig. 3 shows the S, T, and U parameters as functions of the ratio y_2/y_1 in the SDFDM model with $y_1 = 1$. Two sets of m_S and m_D are chosen to separately represent the $m_S < m_D$ and $m_S > m_D$ cases. In the custodial symmetry limits $y_2/y_1 \to \pm 1$, T and U vanish as expected. When $y_2/y_1 \to \pm 2$, S and T become large and will be strongly constrained by EW precision data. U is typically much smaller than the other two parameters, except for some special regions.

In Fig. 4, we show the contours of S, T, and $m_{\chi_1^0}$ in the $m_D - m_S$ plane. Fig. 4(a) corresponds to the custodial symmetry, where T and U are always vanish, and only the behavior of S are demonstrated. In the region with small m_S and m_D, S is an $\mathcal{O}(0.1)$ number, decreasing as m_D increases. This behavior can be understood as follows. For $m_D < m_S \ll yv$ ($y = y_1 = y_2$), the mass spectrum becomes $m_{\chi_1^0} = m_{\chi^\pm} = m_D$, $m_{\chi_{2,3}^0} \approx yv$. Using the expressions (3.23), (3.24), and (3.25), we have

$$\begin{aligned} S &\approx \frac{1}{\pi}\left[\frac{1}{2}J_1'(0, m_D^2, y^2v^2) - \frac{1}{2}J_1'(0, m_D^2, m_D^2) + m_D^2 B_0'(0, m_D^2, m_D^2)\right] \\ &\approx \frac{1}{\pi}\left(\frac{2}{3}\ln\frac{yv}{m_D} - \frac{1}{9}\right), \end{aligned} \tag{3.38}$$

where the leading term $\propto \ln(yv/m_D)$ and becomes smaller as m_D increases.

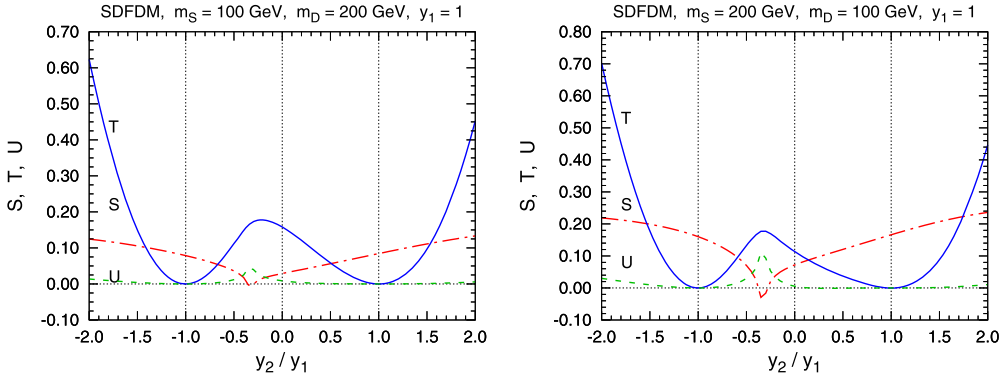

(a) $m_S < m_D$ case (b) $m_S > m_D$ case

Fig. 3. S, T, and U as functions of y_2/y_1 in the SDFDM model with $y_1 = 1$. In the left (right) panel, $m_S = 100$ (200) GeV and $m_D = 200$ (100) GeV.

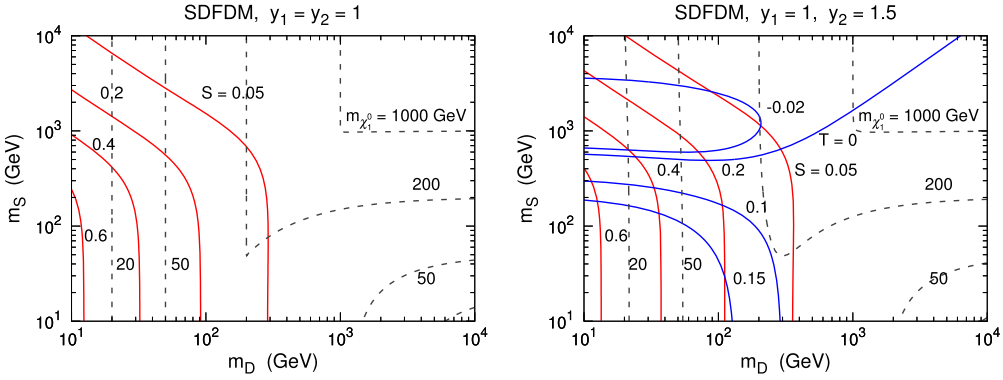

(a) $y_1 = y_2 = 1$ (custodial symmetry) (b) $y_1 = 1$, $y_2 = 1.5$

Fig. 4. Contours of S (red solid lines), T (blue solid lines), and $m_{\chi_1^0}$ (gray dashed lines) in the $m_D - m_S$ plane for the SDFDM model with fixed y_1 and y_2. (For interpretation of the references to color in this figure legend, the reader is referred to the web version of this article.)

Fig. 4(b) demonstrates the effect of custodial symmetry violation with $y_1 = 1$ and $y_2 = 1.5$. T is negative in the region where $m_S > m_D$ with $m_S \gtrsim 600$ GeV. In the region with small m_S and m_D, T is positive and grow quickly as m_D and m_S decrease.

In Fig. 5, we present the expected 95% CL constraints in the $m_D - m_S$ plane from EW oblique parameters after the running of CEPC, as well as that from the current precision. For the custodial symmetry limit $y_1 = y_2$, we use the fit results obtained by assuming $T = U = 0$ and denote the constraints by dotted lines. The solid lines corresponds to the constraints from the global fits under the assumption of $U = 0$, which should be a good approximation for the SDFDM model. The constraints from the global fits with free S, T, and U are indicated by the dot-dashed lines and always weaker than the former constraints.

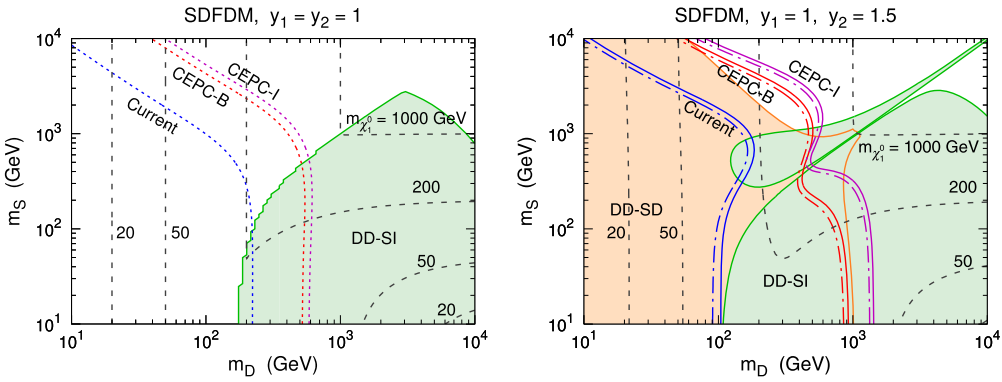

(a) $y_1 = y_2 = 1$ (custodial symmetry) (b) $y_1 = 1$, $y_2 = 1.5$

Fig. 5. Expected 95% CL constraints from CEPC precisions of EW oblique parameters in the $m_D - m_S$ plane for the SDFDM model with fixed y_1 and y_2. The constraints from current, CEPC-B, and CEPC-I precisions are denoted by blue, red, and purple colors, while dotted, solid, and dot-dashed lines correspond to the global fits with $T = U = 0$, $U = 0$, and no constraint on oblique parameters, respectively. The filled orange region is excluded by spin-dependent direct detection (DD-SD), while the filled green region is excluded by the spin-independent direct detection (DD-SI). Gray dashed lines indicate contours of the DM candidate mass $m_{\chi_1^0}$. (For interpretation of the references to color in this figure legend, the reader is referred to the web version of this article.)

For comparison, we also show the constraints from direct detection experiments. The green region denoted as "DD-SI" is excluded by the 90% CL upper limits on the DM-nucleon SI scattering cross section from PandaX-II [81] and LUX [82]. Moreover, the orange region denoted as "DD-SD" is excluded at 90% CL by the upper limit on the DM-neutron SD cross section from LUX [83] and the upper limits on the DM-proton SD cross section from PICO [84].

In Fig. 5(a), the Yukawa couplings are chosen to be $y_1 = y_2 = 1$, respecting the custodial symmetry. In this case, SD direct detection cannot put any bound since $g_{Z\chi_1^0\chi_1^0} = 0$. A large region for $m_D > m_S$ is excluded by SI direct detection. On the other hand, the $m_D < m_S$ half plane evades this constraint because the $h\chi_1^0\chi_1^0$ coupling vanishes. Nevertheless, current EW precision data can test this region up to $m_{\chi_1^0} \sim 200$ GeV, while the running of CEPC is expected to explore up to $m_{\chi_1^0} \sim 600$ GeV.

In Fig. 5(b), we fix $y_1 = 1$ and $y_2 = 1.5$, which do not respect the custodial symmetry. We can find that SI and SD direct detection results collectively exclude a quite large region. Even so, CEPC can still explore further in the parameter space, up to $m_{\chi_1^0} \sim 600$ GeV.

4. Doublet–triplet fermionic dark matter

4.1. Fields and interactions

In the DTFDM model, we consider a dark sector with two doublet and one triplet Weyl spinors [21]:

$$D_1 = \begin{pmatrix} D_1^0 \\ D_1^- \end{pmatrix} \in (\mathbf{2}, -1/2), \quad D_2 = \begin{pmatrix} D_2^+ \\ D_2^0 \end{pmatrix} \in (\mathbf{2}, +1/2), \quad T = \begin{pmatrix} T^+ \\ T^0 \\ T^- \end{pmatrix} \in (\mathbf{3}, 0). \tag{4.1}$$

The related Lagrangians are

$$\mathcal{L}_{\rm D} = i D_1^\dagger \bar\sigma^\mu D_\mu D_1 + i D_2^\dagger \bar\sigma^\mu D_\mu D_2 + (m_D \epsilon_{ij} D_1^i D_2^j + \text{h.c.}), \tag{4.2}$$

$$\mathcal{L}_{\rm T} = i T^\dagger \bar\sigma^\mu D_\mu T - \frac{1}{2}(m_T T^a T^a + \text{h.c.}), \tag{4.3}$$

$$\mathcal{L}_{\rm HDT} = y_1 H_i T^a (\sigma^a)^i_{\ j} D_1^j - y_2 H_i^\dagger T^a (\sigma^a)^i_{\ j} D_2^j + \text{h.c.} \tag{4.4}$$

Triplet interactions with EW gauge bosons can be expressed as

$$\begin{aligned}\mathcal{L}_{\rm T} \supset\ & g[W_\mu^+ (T^+)^\dagger \bar\sigma^\mu T^0 + W_\mu^- (T^0)^\dagger \bar\sigma^\mu T^+ - W_\mu^+ (T^0)^\dagger \bar\sigma^\mu T^- - W_\mu^- (T^-)^\dagger \bar\sigma^\mu T^0] \\ & + (eA_\mu + g c_{\rm W} Z_\mu)(T^+)^\dagger \bar\sigma^\mu T^+ - (eA_\mu + g c_{\rm W} Z_\mu)(T^-)^\dagger \bar\sigma^\mu T^-,\end{aligned} \tag{4.5}$$

while gauge interactions of the doublets have been given by (3.5).

After the Higgs field develops a VEV, we have the mass terms

$$\begin{aligned}\mathcal{L}_{\rm mass} &= -\frac{1}{2}(T^0 \quad D_1^0 \quad D_2^0)\mathcal{M}_{\rm N} \begin{pmatrix} T^0 \\ D_1^0 \\ D_2^0 \end{pmatrix} - (T^- \quad D_1^-)\mathcal{M}_{\rm C} \begin{pmatrix} T^+ \\ D_2^+ \end{pmatrix} + \text{h.c.} \\ &= -\frac{1}{2}\sum_{i=1}^{3} m_{\chi_i^0} \chi_i^0 \chi_i^0 - \sum_{i=1}^{2} m_{\chi_i^\pm} \chi_i^- \chi_i^+ + \text{h.c.}\,,\end{aligned} \tag{4.6}$$

where the mass and mixing matrices are defined as

$$\mathcal{M}_{\rm N} = \begin{pmatrix} m_T & \frac{1}{\sqrt{2}} y_1 v & -\frac{1}{\sqrt{2}} y_2 v \\ \frac{1}{\sqrt{2}} y_1 v & 0 & m_D \\ -\frac{1}{\sqrt{2}} y_2 v & m_D & 0 \end{pmatrix}, \quad \mathcal{M}_{\rm C} = \begin{pmatrix} m_T & -y_2 v \\ -y_1 v & -m_D \end{pmatrix}, \tag{4.7}$$

$$\mathcal{N}^{\rm T} \mathcal{M}_{\rm N} \mathcal{N} = \text{diag}(m_{\chi_1^0}, m_{\chi_2^0}, m_{\chi_3^0}), \quad \mathcal{C}_{\rm R}^{\rm T} \mathcal{M}_{\rm C} \mathcal{C}_{\rm L} = \text{diag}(m_{\chi_1^\pm}, m_{\chi_2^\pm}), \tag{4.8}$$

$$\begin{pmatrix} T^0 \\ D_1^0 \\ D_2^0 \end{pmatrix} = \mathcal{N} \begin{pmatrix} \chi_1^0 \\ \chi_2^0 \\ \chi_3^0 \end{pmatrix}, \quad \begin{pmatrix} T^+ \\ D_2^+ \end{pmatrix} = \mathcal{C}_{\rm L} \begin{pmatrix} \chi_1^+ \\ \chi_2^+ \end{pmatrix}, \quad \begin{pmatrix} T^- \\ D_1^- \end{pmatrix} = \mathcal{C}_{\rm R} \begin{pmatrix} \chi_1^- \\ \chi_2^- \end{pmatrix}. \tag{4.9}$$

The dark sector involves three Majorana fermions $\chi^0_{1,2,3}$ and two singly charged fermion $\chi^\pm_{1,2}$. The couplings of the DM candidate χ_1^0 to the Higgs and Z bosons are

$$g_{h\chi_1^0\chi_1^0} = -\sqrt{2}(y_1 \mathcal{N}_{21} - y_2 \mathcal{N}_{31})\mathcal{N}_{11}, \quad g_{Z\chi_1^0\chi_1^0} = -\frac{g}{2c_{\rm W}}(|\mathcal{N}_{21}|^2 - |\mathcal{N}_{31}|^2). \tag{4.10}$$

These couplings are related to direct detection.

4.2. Vacuum polarizations and custodial symmetry

For evaluating the oblique parameters, we calculate the dark sector contributions to the vacuum polarizations:

$$\Pi_{AA}(p^2) = \frac{2e^2}{16\pi^2}\sum_{i=1}^{2} J_2(p^2, m^2_{\chi_i^\pm}), \tag{4.11}$$

$$\Pi_{ZA}(p^2) = \frac{1}{16\pi^2}\sum_{i=1}^{2} e(a_{Z\chi_i^+\chi_i^-} + b_{Z\chi_i^+\chi_i^-}) J_2(p^2, m^2_{\chi_i^\pm}), \tag{4.12}$$

$$\begin{aligned}\Pi_{ZZ}(p^2) = \frac{1}{16\pi^2}\Bigg\{ &\sum_{i,j=1}^{3}\Big[|g_{Z\chi_i^0\chi_j^0}|^2 J_1(p^2, m^2_{\chi_i^0}, m^2_{\chi_j^0}) \\ &+ m_{\chi_i^0} m_{\chi_j^0}(g^2_{Z\chi_i^0\chi_j^0} + \text{h.c.}) B_0(p^2, m^2_{\chi_i^0}, m^2_{\chi_j^0})\Big] \\ &+ \sum_{i,j=1}^{2}\Big[(|a_{Z\chi_i^+\chi_j^-}|^2 + |b_{Z\chi_i^+\chi_j^-}|^2) J_1(p^2, m^2_{\chi_i^\pm}, m^2_{\chi_j^\pm}) \\ &- 2m_{\chi_i^\pm} m_{\chi_j^\pm}(a_{Z\chi_j^+\chi_i^-} b_{Z\chi_i^+\chi_j^-} + \text{h.c.}) B_0(p^2, m^2_{\chi_i^\pm}, m^2_{\chi_j^\pm})\Big]\Bigg\},\end{aligned} \tag{4.13}$$

$$\begin{aligned}\Pi_{WW}(p^2) = \frac{1}{16\pi^2}\sum_{i=1}^{3}\sum_{j=1}^{2}\Big[&(|a_{W\chi_j^+\chi_i^0}|^2 + |b_{W\chi_j^+\chi_i^0}|^2) J_1(p^2, m^2_{\chi_i^0}, m^2_{\chi_j^\pm}) \\ &- 2m_{\chi_i^0} m_{\chi_j^\pm}(a_{W\chi_j^+\chi_i^0} b^*_{W\chi_j^+\chi_i^0} + \text{h.c.}) B_0(p^2, m^2_{\chi_i^0}, m^2_{\chi_j^\pm})\Big],\end{aligned} \tag{4.14}$$

where the definitions of couplings are

$$a_{Z\chi_i^+\chi_j^-} = g c_{\text{W}} (\mathcal{C}_{\text{L}})^*_{1,i} (\mathcal{C}_{\text{L}})_{1,j} + \frac{g(c^2_{\text{W}} - s^2_{\text{W}})}{2c_{\text{W}}} (\mathcal{C}_{\text{L}})^*_{2,i} (\mathcal{C}_{\text{L}})_{2,j}, \tag{4.15}$$

$$b_{Z\chi_i^+\chi_j^-} = g c_{\text{W}} (\mathcal{C}_{\text{R}})_{1,i} (\mathcal{C}_{\text{R}})^*_{1,j} + \frac{g(c^2_{\text{W}} - s^2_{\text{W}})}{2c_{\text{W}}} (\mathcal{C}_{\text{R}})_{2,i} (\mathcal{C}_{\text{R}})^*_{2,j}, \tag{4.16}$$

$$g_{Z\chi_i^0\chi_j^0} = -\frac{g}{2c_{\text{W}}}(\mathcal{N}_{2,i}\mathcal{N}^*_{2,j} - \mathcal{N}_{3,i}\mathcal{N}^*_{3,j}), \tag{4.17}$$

$$\begin{aligned} a_{W\chi_i^+\chi_j^0} &= g(\mathcal{C}_{\text{L}})^*_{1,i}\mathcal{N}_{1,j} + \frac{g}{\sqrt{2}}(\mathcal{C}_{\text{L}})^*_{2,i}\mathcal{N}_{3,j}, \\ b_{W\chi_i^+\chi_j^0} &= g(\mathcal{C}_{\text{R}})_{1,i}\mathcal{N}^*_{1,j} - \frac{g}{\sqrt{2}}(\mathcal{C}_{\text{R}})_{2,i}\mathcal{N}^*_{2,j}. \end{aligned} \tag{4.18}$$

Analogous to the SDFDM model, the custodial symmetry exists if $y_1 = \pm y_2$, leading to $T = U = 0$ and $g_{Z\chi_1^0\chi_1^0} = 0$. For instance, when $y_1 = y_2 = y$, we can define $\text{SU}(2)_{\text{R}}$ doublets

$$(\mathcal{D}^A)^i = \begin{pmatrix} D_1^i \\ D_2^i \end{pmatrix}, \quad (\mathcal{H}^A)^i = \begin{pmatrix} H_i^\dagger \\ H_i \end{pmatrix}, \tag{4.19}$$

and obtain the $\text{SU}(2)_{\text{L}} \times \text{SU}(2)_{\text{R}}$ invariant Lagrangians

$$\mathcal{L}_{\text{D}} = i\mathcal{D}^\dagger_A \bar{\sigma}^\mu D_\mu \mathcal{D}^A + \frac{1}{2}[m_D \epsilon_{AB}\epsilon_{ij}(\mathcal{D}^A)^i(\mathcal{D}^B)^j + \text{h.c.}], \tag{4.20}$$

$$\mathcal{L}_{\text{HDT}} = y\epsilon_{AB}(\mathcal{H}^A)_i T^a (\sigma^a)^i_j (\mathcal{D}^B)^j + \text{h.c.} \tag{4.21}$$

If $m_D < m_T$, we also have $g_{h\chi_1^0\chi_1^0} = 0$.

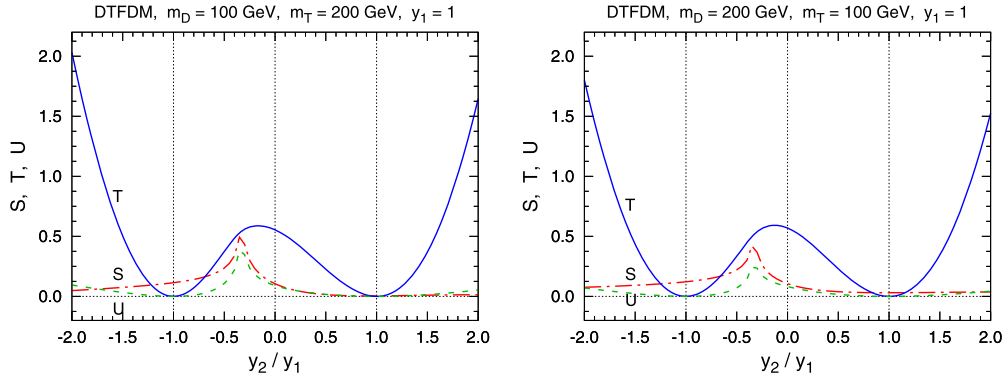

(a) $m_D < m_T$ case (b) $m_D > m_T$ case

Fig. 6. S, T, and U as functions of y_2/y_1 in the DTFDM model with $y_1 = 1$. In the left (right) panel, $m_D =$ 100 (200) GeV and $m_T = 200$ (100) GeV.

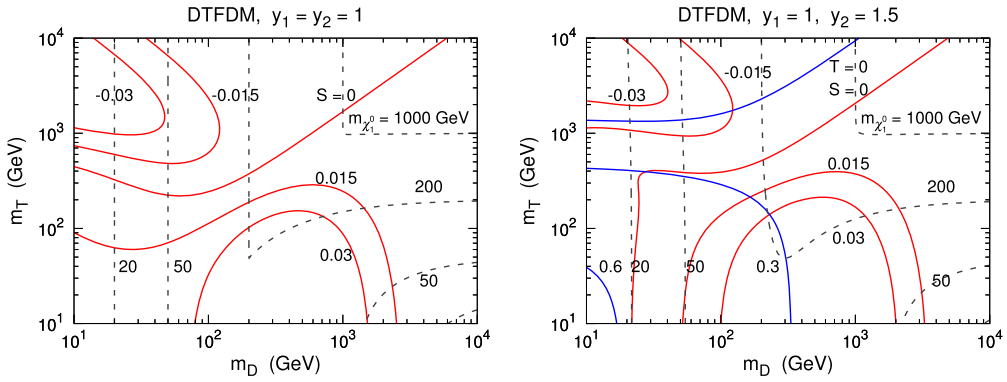

(a) $y_1 = y_2 = 1$ (custodial symmetry) (b) $y_1 = 1$, $y_2 = 1.5$

Fig. 7. Contours of S (red solid lines), T (blue solid lines), and $m_{\chi_1^0}$ (gray dashed lines) in the $m_D - m_T$ plane for the DTFDM model with fixed y_1 and y_2. (For interpretation of the references to color in this figure legend, the reader is referred to the web version of this article.)

4.3. Expected constraints

In Fig. 6, we show the EW oblique parameters as functions of y_2/y_1 in the DTFDM model. T and U vanish at the points respecting the custodial symmetry, *i.e.*, at $y_2/y_1 = \pm 1$. When this symmetry is violated, T increases quickly. S tends to 0 for $0.5 < y_2/y_1 < 2$ in both the $m_D < m_T$ and $m_T < m_D$ cases.

In Fig. 7, we further present the contours of S and T in the $m_D - m_T$ plane. In contrast to the SDFDM model, $|S| \lesssim \mathcal{O}(0.01)$ in these plots, and there are contours corresponding to $S = 0$, separating the regions with different signs of S. An S of $\mathcal{O}(0.01)$ is beyond the reach of current measurements, calling for future CEPC data. For the custodial symmetry limit $y = y_1 = y_2 = 1$, as shown in Fig. 7(a), the masses of dark sector fermions in the region with $m_D < m_T \ll yv$ are $m_{\chi_1^0} = m_D$ and $m_{\chi_{2,3}^0} \approx m_{\chi_{1,2}^\pm} \approx yv$. Thus, we have

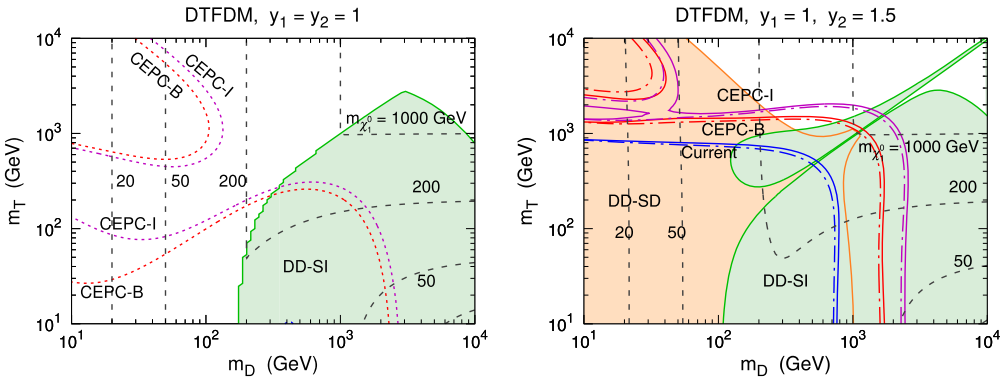

(a) $y_1 = y_2 = 1$ (custodial symmetry) (b) $y_1 = 1$, $y_2 = 1.5$

Fig. 8. Expected 95% CL constraints from CEPC precisions of EW oblique parameters in the $m_D - m_T$ plane for the DTFDM model with fixed y_1 and y_2. The meanings of labels, colors, and line types are the same as in Fig. 5. (For interpretation of the references to color in this figure legend, the reader is referred to the web version of this article.)

$$S \approx \frac{1}{\pi}\left[\frac{1}{2}J_1'(0, m_D^2, y^2v^2) - \frac{1}{2}J_1'(0, y^2v^2, y^2v^2) + 2y^2v^2B_0'(0, y^2v^2, y^2v^2)\right] \approx \frac{1}{18\pi}, \tag{4.22}$$

which explains the $\mathcal{O}(0.01)$ magnitude of S.

The key to obtain the approximation (3.38) in the SDSDM model is that there is an unmixed charged particle which has a mass m_D. This brings us a $J_1(0, m_D^2, m_D^2)$ term which contains a $\ln(m_D^2/Q^2)$ contribution to Π_{ZZ}. After taking into account the first term $J_1'(0, m_D^2, y^2v^2)$ that involves a $\ln(y^2v^2/Q^2)$ term, we have a significant $\ln(y^2v^2/m_D^2)$ contribution to S in the end. On the order hand, the two charged fermions in the DTFDM model mix up and both their masses tend to yv when $m_D \ll yv$. Consequently, their contribution to Π_{ZZ} leads to a $J_1(0, y^2v^2, y^2v^2)$ term, which involve a $\ln(y^2v^2/Q^2)$ term that is canceled by the first term $J_1'(0, m_D^2, y^2v^2)$. Therefore, there is no significant logarithmic contribution any more, leading to a much smaller S.

Fig. 7(b) corresponds the case violating the custodial symmetry, where the T parameter turns on. We fix $y_1 = 1$ and $y_2 = 1.5$ fixed and find that T is negative in a region where $m_T > m_D$ and $m_T \gtrsim 1$ TeV. For small m_D and m_T, T is positive and grows fast as m_D and m_T decrease. For large m_D and m_T, S has similar values to the custodial symmetric case. For very small mass parameters, however, it becomes negative.

Expected constraints from the CEPC determination of EW oblique parameters and current bounds from direct detection on the DTFDM model in the $m_D - m_T$ plane are shown in Fig. 8. The DD-SI and DD-SD exclusion regions are very similar to those in the SDFDM model. Nevertheless, for the reason discussed above, the expected constraints from EW data are quite different. As shown in Fig. 8(a) for the custodial symmetry limit $y_1 = y_2 = 1$, current EW precision measurements are not sensitive at all. CEPC data are sensitive to two separate regions, but a large portion of parameter space with moderate mass parameters cannot be explored. For the case with $y_1 = 1$ and $y_2 = 1.5$ in Fig. 8(b), CEPC measurements can probe up to $m_{\chi_1^0} \sim 2$ TeV, but only a small portion of the CEPC-sensitive region is not excluded by current direct experiments.

5. Triplet–quadruplet fermionic dark matter

5.1. Fields and interactions

In the TQFDM model, one triplet and two quadruplet Weyl spinors are introduced [26]:

$$T=\begin{pmatrix}T^+\\T^0\\T^-\end{pmatrix}\in(\mathbf{3},0),\quad Q_1=\begin{pmatrix}Q_1^+\\Q_1^0\\Q_1^-\\Q_1^{--}\end{pmatrix}\in(\mathbf{4},-1/2),\quad Q_2=\begin{pmatrix}Q_2^{++}\\Q_2^+\\Q_2^0\\Q_2^-\end{pmatrix}\in(\mathbf{4},+1/2). \tag{5.1}$$

Their properties are described by the Lagrangians

$$\mathcal{L}_{\mathrm{T}}=iT^\dagger\bar\sigma^\mu D_\mu T-\frac{1}{2}(m_T T^a T^a+\mathrm{h.c.}), \tag{5.2}$$

$$\mathcal{L}_{\mathrm{Q}}=iQ_1^\dagger\bar\sigma^\mu D_\mu Q_1+iQ_2^\dagger\bar\sigma^\mu D_\mu Q_2-(m_Q Q_1 Q_2+\mathrm{h.c.}), \tag{5.3}$$

$$\mathcal{L}_{\mathrm{HTQ}}=y_1 Q_1 T H-y_2 Q_2 T H^\dagger+\mathrm{h.c.}, \tag{5.4}$$

where

$$Q_1 T H=\epsilon_{jl}(Q_1)_i^{jk}T_k^i H^l\to\left(\frac{1}{\sqrt{3}}Q_1^- T^+-\frac{2}{\sqrt{6}}Q_1^0 T^0-Q_1^+ T^-\right)\frac{v+h}{\sqrt{2}}, \tag{5.5}$$

$$Q_2 T H^\dagger=(Q_1)_i^{jk}T_k^i H_j^\dagger\to\left(-\frac{2}{\sqrt{6}}Q_2^0 T^0-\frac{1}{\sqrt{3}}Q_2^+ T^-+Q_2^- T^+\right)\frac{v+h}{\sqrt{2}}. \tag{5.6}$$

Gauge interactions of the quadruplets can be derived as

$$\begin{aligned}\mathcal{L}_{\mathrm{Q}}\supset&\left\{\frac{\sqrt{6}}{2}gW_\mu^+[(Q_1^+)^\dagger\bar\sigma^\mu Q_1^0+(Q_2^{++})^\dagger\bar\sigma^\mu Q_2^+ +(Q_1^-)^\dagger\bar\sigma^\mu Q_1^{--}+(Q_2^0)^\dagger\bar\sigma^\mu Q_2^-]\right.\\&\left.+\sqrt{2}gW_\mu^+[(Q_1^0)^\dagger\bar\sigma^\mu Q_1^-+(Q_2^+)^\dagger\bar\sigma^\mu Q_2^0]+\mathrm{h.c.}\right\}\\&+\left[eA_\mu+\frac{g(s_{\mathrm{W}}^2+3c_{\mathrm{W}}^2)}{2c_{\mathrm{W}}}Z_\mu\right](Q_1^+)^\dagger\bar\sigma^\mu Q_1^+\\&+\left[eA_\mu+\frac{g(c_{\mathrm{W}}^2-s_{\mathrm{W}}^2)}{2c_{\mathrm{W}}}Z_\mu\right](Q_2^+)^\dagger\bar\sigma^\mu Q_2^+\\&+\frac{g}{2c_{\mathrm{W}}}Z_\mu(Q_1^0)^\dagger\bar\sigma^\mu Q_1^0+\left[2eA_\mu+\frac{g(3c_{\mathrm{W}}^2-s_{\mathrm{W}}^2)}{2c_{\mathrm{W}}}Z_\mu\right](Q_2^{++})^\dagger\bar\sigma^\mu Q_2^{++}\\&-\left[eA_\mu+\frac{g(3c_{\mathrm{W}}^2+s_{\mathrm{W}}^2)}{2c_{\mathrm{W}}}Z_\mu\right](Q_2^-)^\dagger\bar\sigma^\mu Q_2^-\\&-\left[eA_\mu+\frac{g(c_{\mathrm{W}}^2-s_{\mathrm{W}}^2)}{2c_{\mathrm{W}}}Z_\mu\right](Q_1^-)^\dagger\bar\sigma^\mu Q_1^-\\&-\frac{g}{2c_{\mathrm{W}}}Z_\mu(Q_2^0)^\dagger\bar\sigma^\mu Q_2^0-\left[2eA_\mu+\frac{g(3c_{\mathrm{W}}^2-s_{\mathrm{W}}^2)}{2c_{\mathrm{W}}}Z_\mu\right](Q_1^{--})^\dagger\bar\sigma^\mu Q_1^{--}.\end{aligned} \tag{5.7}$$

Gauge interactions of the triplet are the same as in (4.5).

Mass terms in the dark sector are

$$\begin{aligned}\mathcal{L}_{\rm mass} &= -\frac{1}{2}(T^0 \quad Q_1^0 \quad Q_2^0)\mathcal{M}_{\rm N}\begin{pmatrix} T^0 \\ Q_1^0 \\ Q_2^0 \end{pmatrix} - (T^- \quad Q_1^- \quad Q_2^-)\mathcal{M}_{\rm C}\begin{pmatrix} T^+ \\ Q_1^+ \\ Q_2^+ \end{pmatrix} \\ &\quad - m_Q Q_1^{--} Q_2^{++} + \text{h.c.} \\ &= -\frac{1}{2}\sum_{i=1}^{3} m_{\chi_i^0}\chi_i^0\chi_i^0 - \sum_{i=1}^{3} m_{\chi_i^\pm}\chi_i^-\chi_i^+ - m_{\chi^{\pm\pm}}\chi^{--}\chi^{++} + \text{h.c.}\,, \end{aligned} \tag{5.8}$$

where $m_{\chi^{\pm\pm}} = m_Q$, $\chi^{--} = Q_1^{--}$, $\chi^{++} = Q_2^{++}$, and the definitions of the mass and mixing matrices are

$$\begin{aligned}\mathcal{M}_{\rm N} &= \begin{pmatrix} m_T & \frac{1}{\sqrt{3}}y_1 v & -\frac{1}{\sqrt{3}}y_2 v \\ \frac{1}{\sqrt{3}}y_1 v & 0 & m_Q \\ -\frac{1}{\sqrt{3}}y_2 v & m_Q & 0 \end{pmatrix}, \\ \mathcal{M}_{\rm C} &= \begin{pmatrix} m_T & \frac{1}{\sqrt{2}}y_1 v & -\frac{1}{\sqrt{6}}y_2 v \\ -\frac{1}{\sqrt{6}}y_1 v & 0 & -m_Q \\ \frac{1}{\sqrt{2}}y_2 v & -m_Q & 0 \end{pmatrix}, \end{aligned} \tag{5.9}$$

$$\mathcal{N}^{\rm T}\mathcal{M}_{\rm N}\mathcal{N} = \text{diag}(m_{\chi_1^0}, m_{\chi_2^0}, m_{\chi_3^0}), \quad \mathcal{C}_{\rm R}^{\rm T}\mathcal{M}_{\rm C}\mathcal{C}_{\rm L} = \text{diag}(m_{\chi_1^\pm}, m_{\chi_2^\pm}, m_{\chi_2^\pm}), \tag{5.10}$$

$$\begin{pmatrix} T^0 \\ Q_1^0 \\ Q_2^0 \end{pmatrix} = \mathcal{N}\begin{pmatrix} \chi_1^0 \\ \chi_2^0 \\ \chi_3^0 \end{pmatrix}, \quad \begin{pmatrix} T^+ \\ Q_1^+ \\ Q_2^+ \end{pmatrix} = \mathcal{C}_{\rm L}\begin{pmatrix} \chi_1^+ \\ \chi_2^+ \\ \chi_3^+ \end{pmatrix}, \quad \begin{pmatrix} T^- \\ Q_1^- \\ Q_2^- \end{pmatrix} = \mathcal{C}_{\rm R}\begin{pmatrix} \chi_1^- \\ \chi_2^- \\ \chi_3^- \end{pmatrix}. \tag{5.11}$$

There are three Majorana fermions $\chi_{1,2,3}^0$, three singly charged fermions $\chi_{1,2,3}^\pm$, and one doubly charged fermion $\chi^{\pm\pm}$. The DM candidate χ_1^0 has trilinear couplings to the Higgs and Z bosons:

$$g_{h\chi_1^0\chi_1^0} = -\frac{2}{\sqrt{3}}(y_1\mathcal{N}_{21} - y_2\mathcal{N}_{31})\mathcal{N}_{11}, \quad g_{Z\chi_1^0\chi_1^0} = -\frac{g}{2c_{\rm W}}(|\mathcal{N}_{21}|^2 - |\mathcal{N}_{31}|^2). \tag{5.12}$$

Therefore, it may induce signals in direct detection experiments.

5.2. Vacuum polarizations and custodial symmetry

The vacuum polarizations of EW gauge bosons contributed by dark sector fermions can be expressed as

$$\Pi_{AA}(p^2) = \frac{2e^2}{16\pi^2}\sum_{i=1}^{3} J_2(p^2, m_{\chi_i^\pm}^2) + \frac{8e^2}{16\pi^2}J_2(p^2, m_{\chi^{\pm\pm}}^2), \tag{5.13}$$

$$\Pi_{ZA}(p^2) = \frac{1}{16\pi^2}\sum_{i=1}^{3} e(a_{Z\chi_i^+\chi_i^-} + b_{Z\chi_i^+\chi_i^-}) J_2(p^2, m^2_{\chi_i^\pm}) + \frac{2eg}{16\pi^2}\frac{3c_{\rm W}^2 - s_{\rm W}^2}{c_{\rm W}} J_2(p^2, m^2_{\chi^{\pm\pm}}), \tag{5.14}$$

$$\begin{aligned}\Pi_{ZZ}(p^2) = \frac{1}{16\pi^2}\Bigg\{ &\sum_{i,j=1}^{3}\Big[|g_{Z\chi_i^0\chi_j^0}|^2 J_1(p^2, m^2_{\chi_i^0}, m^2_{\chi_j^0}) \\ &+ m_{\chi_i^0} m_{\chi_j^0}(g^2_{Z\chi_i^0\chi_j^0} + \text{h.c.}) B_0(p^2, m^2_{\chi_i^0}, m^2_{\chi_j^0})\Big] \\ &+ \sum_{i,j=1}^{3}\Big[(|a_{Z\chi_i^+\chi_j^-}|^2 + |b_{Z\chi_i^+\chi_j^-}|^2) J_1(p^2, m^2_{\chi_i^\pm}, m^2_{\chi_j^\pm}) \\ &- 2m_{\chi_i^\pm} m_{\chi_j^\pm}(a_{Z\chi_j^+\chi_i^-} b_{Z\chi_i^+\chi_j^-} + \text{h.c.}) B_0(p^2, m^2_{\chi_i^\pm}, m^2_{\chi_j^\pm})\Big] \\ &+ \frac{g^2(3c_{\rm W}^2 - s_{\rm W}^2)^2}{c_{\rm W}^2} J_2(p^2, m^2_{\chi^{\pm\pm}})\Bigg\},\end{aligned} \tag{5.15}$$

$$\begin{aligned}\Pi_{WW}(p^2) = \frac{1}{16\pi^2}\Bigg\{ &\sum_{i,j=1}^{3}\Big[(|a_{W\chi_j^+\chi_i^0}|^2 + |b_{W\chi_j^+\chi_i^0}|^2) J_1(p^2, m^2_{\chi_i^0}, m^2_{\chi_j^\pm}) \\ &- 2m_{\chi_i^0} m_{\chi_j^\pm}(a_{W\chi_j^+\chi_i^0} b^*_{W\chi_j^+\chi_i^0} + \text{h.c.}) B_0(p^2, m^2_{\chi_i^0}, m^2_{\chi_j^\pm})\Big] \\ &+ \sum_{i=1}^{3}\Big[(|a_{W\chi^{++}\chi_i^+}|^2 + |b_{W\chi^{++}\chi_i^+}|^2) J_1(p^2, m^2_{\chi_i^\pm}, m^2_{\chi^{\pm\pm}}) \\ &- 2m_{\chi^{\pm\pm}} m_{\chi_i^\pm}(a_{W\chi^{++}\chi_i^+} b^*_{W\chi^{++}\chi_i^+} + \text{h.c.}) B_0(p^2, m^2_{\chi_i^\pm}, m^2_{\chi^{\pm\pm}})\Big]\Bigg\},\end{aligned} \tag{5.16}$$

where the related couplings are

$$a_{Z\chi_i^+\chi_j^-} = gc_{\rm W}(\mathcal{C}_{\rm L})^*_{1,i}(\mathcal{C}_{\rm L})_{1,j} + \frac{g(3c_{\rm W}^2 + s_{\rm W}^2)}{2c_{\rm W}}(\mathcal{C}_{\rm L})^*_{2,i}(\mathcal{C}_{\rm L})_{2,j} + \frac{g(c_{\rm W}^2 - s_{\rm W}^2)}{2c_{\rm W}}(\mathcal{C}_{\rm L})^*_{3,i}(\mathcal{C}_{\rm L})_{3,j}, \tag{5.17}$$

$$b_{Z\chi_i^+\chi_j^-} = gc_{\rm W}(\mathcal{C}_{\rm R})_{1,i}(\mathcal{C}_{\rm R})^*_{1,j} + \frac{g(c_{\rm W}^2 - s_{\rm W}^2)}{2c_{\rm W}}(\mathcal{C}_{\rm R})_{2,i}(\mathcal{C}_{\rm R})^*_{2,j} + \frac{g(3c_{\rm W}^2 + s_{\rm W}^2)}{2c_{\rm W}}(\mathcal{C}_{\rm R})_{3,i}(\mathcal{C}_{\rm R})^*_{3,j}, \tag{5.18}$$

$$g_{Z\chi_i^0\chi_j^0} = -\frac{g}{2c_{\rm W}}(\mathcal{N}_{2,i}\mathcal{N}^*_{2,j} - \mathcal{N}_{3,i}\mathcal{N}^*_{3,j}), \tag{5.19}$$

$$a_{W\chi_i^+\chi_j^0} = g(\mathcal{C}_{\rm L})^*_{1,i}\mathcal{N}_{1,j} + \frac{\sqrt{6}}{2}g(\mathcal{C}_{\rm L})^*_{2,i}\mathcal{N}_{2,j} + \sqrt{2}g(\mathcal{C}_{\rm L})^*_{3,i}\mathcal{N}_{3,j}, \tag{5.20}$$

$$b_{W\chi_i^+\chi_j^0} = g(\mathcal{C}_{\rm R})_{1,i}\mathcal{N}^*_{1,j} - \sqrt{2}g(\mathcal{C}_{\rm R})_{2,i}\mathcal{N}^*_{2,j} - \frac{\sqrt{6}}{2}g(\mathcal{C}_{\rm R})_{3,i}\mathcal{N}^*_{3,j}. \tag{5.21}$$

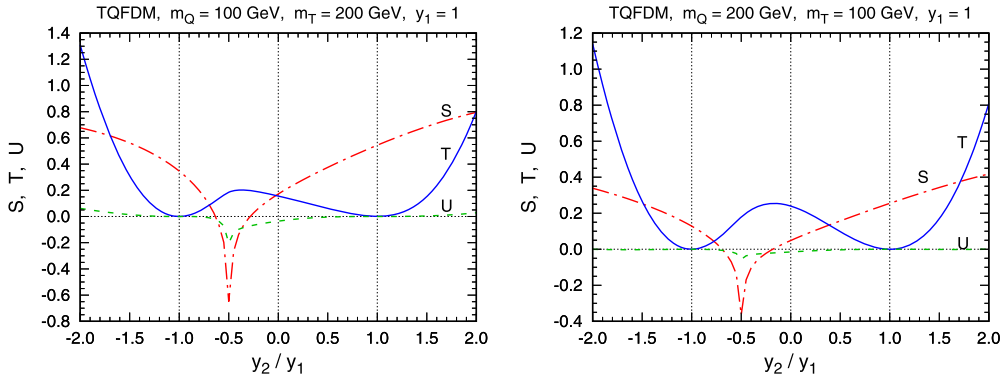

(a) $m_Q < m_T$ case (b) $m_Q > m_T$ case

Fig. 9. S, T, and U as functions of y_2/y_1 in the TQFDM model with $y_1 = 1$. In the left (right) panel, $m_Q =$ 100 (200) GeV and $m_T = 200$ (100) GeV.

Similar to the SDFDM and DTFDM models, $y_1 = \pm y_2$ leads to the custodial symmetry, and hence $T = U = g_{Z\chi_1^0\chi_1^0} = 0$. For $y_1 = y_2 = y$, $\mathrm{SU}(2)_\mathrm{R}$ doublets

$$(\mathcal{Q}^A)_k^{ij} = \begin{pmatrix} (Q_1)_k^{ij} \\ (Q_2)_k^{ij} \end{pmatrix}, \quad (\mathcal{H}^A)^i = \begin{pmatrix} H_i^\dagger \\ H_i \end{pmatrix}, \tag{5.22}$$

can be used to manifest $\mathrm{SU}(2)_\mathrm{L} \times \mathrm{SU}(2)_\mathrm{R}$ invariant Lagrangians

$$\mathcal{L}_\mathrm{Q} = i\mathcal{Q}_A^\dagger \bar{\sigma}^\mu D_\mu \mathcal{Q}^A - \frac{1}{2}[m_Q \epsilon_{AB}\epsilon_{il}(\mathcal{Q}^A)_k^{ij}(\mathcal{Q}^B)_j^{lk} + \mathrm{h.c.}], \tag{5.23}$$

$$\mathcal{L}_\mathrm{HTQ} = y\epsilon_{AB}(\mathcal{Q}^A)_i^{jk} T_k^i (\mathcal{H}^B)_j + \mathrm{h.c.} \tag{5.24}$$

In this case, $g_{h\chi_1^0\chi_1^0} = 0$ holds for $m_Q < m_T$, leading to a vanishing SI DM-nucleon scattering cross section at tree level.

5.3. Expected constraints

We demonstrate the behaviors of EW oblique parameters as functions of y_2/y_1 for the TQFDM model with fixed mass parameters in Fig. 9. For $y_2/y_1 = \pm 1$, T and U arrive at zero, due to the custodial symmetry. The S parameter has a dip at $y_2/y_1 \approx -0.5$, where $m_{\chi_1^0}$ and $m_{\chi_1^\pm}$ approach to zero, leading to large contributions to vacuum polarizations.

Fig. 10 exhibits the contours of S and T in the $m_Q - m_T$ plane with fixed Yukawa couplings. The behaviors of S and T are quite similar to those in the SDFDM model, but the values of S are larger, since the gauge interactions are stronger. For the custodial symmetry limit $y_1 = y_2 = 1$, which corresponds to Fig. 10(a), we can have an approximate analysis on S, analogous to that in Subsection 3.3. When $m_Q < m_T \ll yv$, the mass spectrum is $m_{\chi_1^0} = m_{\chi_1^\pm} = m_{\chi^{\pm\pm}} = m_Q$, $m_{\chi_{2,3}^0} \approx m_{\chi_{2,3}^\pm} \approx \sqrt{6}yv/3$, resulting in a significant $\ln(yv/m_Q)$ term for S. We can conclude that the similar behaviors of S in the SDFDM and TQFDM models is because there is an unmixed particle, either $\chi^\pm$ or $\chi^{\pm\pm}$. In contrast, dark sector fermions are all mixed with each other in the DTFDM model, producing a very different behavior. For $y_1 = 1$ and $y_2 = 1.5$, which corresponds

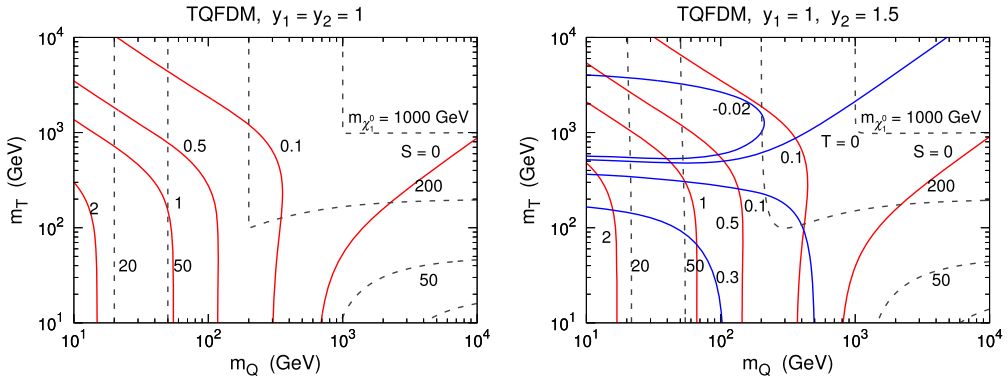

(a) $y_1 = y_2 = 1$ (custodial symmetry) (b) $y_1 = 1$, $y_2 = 1.5$

Fig. 10. Contours of S (red solid lines), T (blue solid lines), and $m_{\chi_1^0}$ (gray dashed lines) in the $m_Q - m_T$ plane for the TQFDM model with fixed y_1 and y_2. (For interpretation of the references to color in this figure legend, the reader is referred to the web version of this article.)

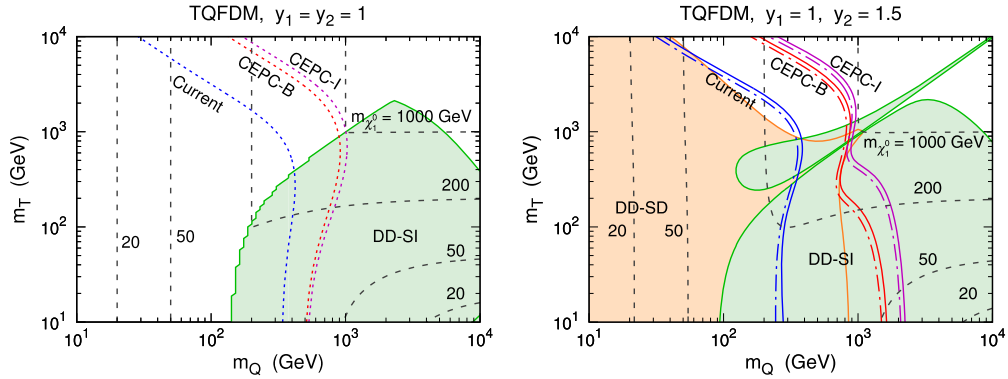

(a) $y_1 = y_2 = 1$ (custodial symmetry) (b) $y_1 = 1$, $y_2 = 1.5$

Fig. 11. Expected 95% CL constraints from CEPC precisions of EW oblique parameters in the $m_Q - m_T$ plane for the TQFDM model with fixed y_1 and y_2. The meanings of labels, colors, and line types are the same as in Fig. 5. (For interpretation of the references to color in this figure legend, the reader is referred to the web version of this article.)

to Fig. 10(b), not only the behavior of T but also the values are analogous to those in the SDFDM model.

In Fig. 11, we show both the expected constraints from oblique parameters and the current direct detection bounds in the $m_Q - m_T$ plane. The exclusion regions from direct detection are quite analogous to those in the SDFDM and DTFDM models, since the intrinsic physics is basically identical. Moreover, the limits from EW precision measurements have similar behaviors to those in the SDFDM model, due to the reason discussed above. But the expected exclusion regions are enlarged. For both the case of $y_1 = y_2 = 1$ in Fig. 11(a) and the case of $y_1 = 1$ and $y_2 = 1.5$ in Fig. 11(b), CEPC EW data could explore up to $m_{\chi_1^0} \sim 1$ TeV.

6. Conclusions and discussions

The future CEPC project will greatly improve EW precision measurements, leading to an unprecedented precision of EW oblique parameters. This will provide an excellent opportunity to indirectly test new physics with EW interactions, in particular, WIMP dark matter. In this work, we calculate the expected constraints from CEPC EW data on fermionic WIMP dark matter. Current direct detection bounds are also demonstrated for comparison.

The expected CEPC precisions of oblique parameters are derived through global fits assuming reduction of the uncertainties of EW precision observables due to future CEPC data and theoretical efforts. Fit results are obtained for the case where all the oblique parameters are free and for the cases assuming some of them vanish. We have used these results to study the CEPC sensitivity to three WIMP models, *i.e.*, the SDFDM, DTFDM, and TQFDM models.

Each of these models has a dark sector consisting of fermionic multiplets in two $SU(2)_L$ representations whose dimensions differ by one and allow two kinds of Yukawa couplings to the SM Higgs doublet. The DM candidate χ_1^0 is the lightest mass eigenstate of multiplet neutral components. When the two Yukawa couplings are equal, there is a custodial symmetry resulting in vanishing DM couplings to the Higgs and Z bosons in a particular region of the parameter space. In this case, direct detection experiments can hardly probe the model, while CEPC EW data would still be very sensitive. Moreover, in the case with custodial symmetry violation, CEPC can also explore further than current direct detection. In some moderate values of Yukawa couplings, we find that CEPC data are expected to probe up to $m_{\chi_1^0} \sim 600$ GeV, 2 TeV, and 1 TeV in the SDFDM, DTFDM, and TQFDM models, respectively.

LHC searches for production of dark sector fermions are also important for studying these models. Nevertheless, the LHC sensitivity is limited by the low electroweak production rates and complicated final states. Since CEPC EW data can reach up to TeV mass scales, as shown above, the CEPC sensitivity could be much better than LHC. It is worth emphasizing that collider studies on dark matter are free from astrophysical and cosmological factors, only depending on its properties in particle physics.

In contrast, the interpretations of direct and indirect detection experimental results depend on many astrophysical inputs, *e.g.*, the local DM density, J-factors of dwarf galaxies, and ambiguous astrophysical backgrounds. The information inferred from the observed DM relic abundance is not totally solid, since the calculation may be affected by nonstandard cosmological evolution. Therefore, collider studies should be treated as an independent and robust way for exploring DM particle nature.

Acknowledgements

We thank Bin Zhu, Dan-Yang Liu, and Zhong-Hui Zhang for discussions. This work is supported by the National Natural Science Foundation of China (NSFC) under Grant Nos. 11375277, 11410301005, 11647606 and 11005163, the Fundamental Research Funds for the Central Universities, the Natural Science Foundation of Guangdong Province under Grant No. 2016A030313313, and the Sun Yat-Sen University Science Foundation. ZHY is supported by the Australian Research Council.

Appendix A. Dark matter scattering off nucleons

In the SDFDM, DTFDM, and TQFDM models, the DM candidate χ_1^0 may have nonzero couplings to the Higgs and Z bosons. The exchange of a Higgs boson between χ_1^0 and nuclei leads to SI scattering, while the exchange of a Z boson leads to SD scattering. Therefore, direct detection experiments have potential to explore these models. In this appendix, we provide the expressions for calculating the scattering cross sections.

The Lagrangian for the trilinear interaction between the Majorana fermion χ_1^0 and the Higgs boson is given by Eq. (3.9). For zero momentum transfer, it induces an effective operator describing the scalar interaction between χ_1^0 and a nucleon N:

$$\mathcal{L}_{\mathrm{S},N} = \sum_{N=p,n} G_{\mathrm{S},N} \bar{\chi}_1^0 \chi_1^0 \bar{N} N, \tag{A.1}$$

with

$$G_{\mathrm{S},N} = -\frac{g_{h\chi_1^0\chi_1^0} m_N}{2v m_h^2} \left(\sum_{q=u,d,s} f_q^N + 3 f_Q^N \right). \tag{A.2}$$

The nucleon form factors f_i^N are given by [85]

$$f_u^p = 0.020 \pm 0.004, \quad f_d^p = 0.026 \pm 0.005, \quad f_u^n = 0.014 \pm 0.003, \tag{A.3}$$

$$f_d^n = 0.036 \pm 0.008, \quad f_s^p = f_s^n = 0.118 \pm 0.062, \quad f_Q^N = \frac{2}{27} \left(1 - \sum_{q=u,d,s} f_q^N \right). \tag{A.4}$$

The SI scattering cross section due to this effective interaction can be expressed as [86]

$$\sigma_{\chi N}^{\mathrm{SI}} = \frac{4}{\pi} \mu_{\chi N}^2 G_{\mathrm{S},N}^2, \tag{A.5}$$

where $\mu_{\chi N} \equiv m_{\chi_1^0} m_N / (m_{\chi_1^0} + m_N)$ is the reduced mass.

The Lagrangian for the trilinear interaction between χ_1^0 and the Z boson is given by Eq. (3.11). It leads to an effective operator for the axial vector interaction:

$$\mathcal{L}_{\mathrm{A},N} = \sum_{N=p,n} G_{\mathrm{A},N} \bar{\chi}_1^0 \gamma^\mu \gamma_5 \chi_1^0 \bar{N} \gamma_\mu \gamma_5 N, \tag{A.6}$$

with

$$G_{\mathrm{A},N} = \sum_{q=u,d,s} G_{\mathrm{A},q} \Delta_q^N, \quad G_{\mathrm{A},q} = \frac{g g_{\mathrm{A}}^q g_{Z\chi_1^0\chi_1^0}}{4 c_{\mathrm{W}} m_Z^2}, \tag{A.7}$$

where $g_{\mathrm{A}}^u = 1/2$, $g_{\mathrm{A}}^d = g_{\mathrm{A}}^s = -1/2$, and the form factors are [87]

$$\Delta_u^p = \Delta_d^n = 0.842 \pm 0.012, \quad \Delta_d^p = \Delta_u^n = -0.427 \pm 0.013,$$
$$\Delta_s^p = \Delta_s^n = -0.085 \pm 0.018. \tag{A.8}$$

This effective interaction induces SD scattering with a cross section [86]

$$\sigma_{\chi N}^{\mathrm{SD}} = \frac{12}{\pi} \mu_{\chi N}^2 G_{\mathrm{A},N}^2. \tag{A.9}$$

References

[1] G. Jungman, M. Kamionkowski, K. Griest, Supersymmetric dark matter, Phys. Rep. 267 (1996) 195–373, arXiv:hep-ph/9506380.
[2] G. Bertone, D. Hooper, J. Silk, Particle dark matter: evidence, candidates and constraints, Phys. Rep. 405 (2005) 279–390, arXiv:hep-ph/0404175.
[3] J.L. Feng, Dark matter candidates from particle physics and methods of detection, Annu. Rev. Astron. Astrophys. 48 (2010) 495–545, arXiv:1003.0904.
[4] H. Goldberg, Constraint on the photino mass from cosmology, Phys. Rev. Lett. 50 (1983) 1419.
[5] J.R. Ellis, J.S. Hagelin, D.V. Nanopoulos, K.A. Olive, M. Srednicki, Supersymmetric relics from the big bang, Nucl. Phys. B 238 (1984) 453–476.
[6] G. Servant, T.M.P. Tait, Is the lightest Kaluza–Klein particle a viable dark matter candidate?, Nucl. Phys. B 650 (2003) 391–419, arXiv:hep-ph/0206071.
[7] H.-C. Cheng, J.L. Feng, K.T. Matchev, Kaluza–Klein dark matter, Phys. Rev. Lett. 89 (2002) 211301, arXiv:hep-ph/0207125.
[8] M. Cirelli, N. Fornengo, A. Strumia, Minimal dark matter, Nucl. Phys. B 753 (2006) 178–194, arXiv:hep-ph/0512090.
[9] M. Cirelli, A. Strumia, M. Tamburini, Cosmology and astrophysics of minimal dark matter, Nucl. Phys. B 787 (2007) 152–175, arXiv:0706.4071.
[10] M. Cirelli, A. Strumia, Minimal dark matter: model and results, New J. Phys. 11 (2009) 105005, arXiv:0903.3381.
[11] T. Hambye, F.S. Ling, L. Lopez Honorez, J. Rocher, Scalar multiplet dark matter, J. High Energy Phys. 07 (2009) 090, arXiv:0903.4010.
[12] Y. Cai, W. Chao, S. Yang, Scalar septuplet dark matter and enhanced $h \to \gamma\gamma$ decay rate, J. High Energy Phys. 12 (2012) 043, arXiv:1208.3949.
[13] B. Ostdiek, Constraining the minimal dark matter fiveplet with LHC searches, Phys. Rev. D 92 (2015) 055008, arXiv:1506.03445.
[14] C. Cai, Z.-M. Huang, Z. Kang, Z.-H. Yu, H.-H. Zhang, Perturbativity limits for scalar minimal dark matter with Yukawa interactions: septuplet, Phys. Rev. D 92 (2015) 115004, arXiv:1510.01559.
[15] R. Mahbubani, L. Senatore, The Minimal model for dark matter and unification, Phys. Rev. D 73 (2006) 043510, arXiv:hep-ph/0510064.
[16] F. D'Eramo, Dark matter and Higgs boson physics, Phys. Rev. D 76 (2007) 083522, arXiv:0705.4493.
[17] R. Enberg, P.J. Fox, L.J. Hall, A.Y. Papaioannou, M. Papucci, LHC and dark matter signals of improved naturalness, J. High Energy Phys. 11 (2007) 014, arXiv:0706.0918.
[18] T. Cohen, J. Kearney, A. Pierce, D. Tucker-Smith, Singlet–doublet dark matter, Phys. Rev. D 85 (2012) 075003, arXiv:1109.2604.
[19] O. Fischer, J.J. van der Bij, The scalar singlet–triplet dark matter model, J. Cosmol. Astropart. Phys. 1401 (2014) 032, arXiv:1311.1077.
[20] C. Cheung, D. Sanford, Simplified models of mixed dark matter, J. Cosmol. Astropart. Phys. 1402 (2014) 011, arXiv:1311.5896.
[21] A. Dedes, D. Karamitros, Doublet–triplet fermionic dark matter, Phys. Rev. D 89 (2014) 115002, arXiv:1403.7744.
[22] L. Calibbi, A. Mariotti, P. Tziveloglou, Singlet–doublet model: dark matter searches and LHC constraints, J. High Energy Phys. 10 (2015) 116, arXiv:1505.03867.
[23] A. Freitas, S. Westhoff, J. Zupan, Integrating in the Higgs portal to fermion dark matter, J. High Energy Phys. 09 (2015) 015, arXiv:1506.04149.
[24] M.A. Fedderke, T. Lin, L.-T. Wang, Probing the fermionic Higgs portal at lepton colliders, J. High Energy Phys. 04 (2016) 160, arXiv:1506.05465.
[25] C.E. Yaguna, Singlet–doublet Dirac dark matter, Phys. Rev. D 92 (2015) 115002, arXiv:1510.06151.
[26] T.M.P. Tait, Z.-H. Yu, Triplet–quadruplet dark matter, J. High Energy Phys. 03 (2016) 204, arXiv:1601.01354.
[27] S. Horiuchi, O. Macias, D. Restrepo, A. Rivera, O. Zapata, H. Silverwood, The Fermi-LAT gamma–ray excess at the Galactic Center in the singlet–doublet fermion dark matter model, J. Cosmol. Astropart. Phys. 1603 (2016) 048, arXiv:1602.04788.
[28] S. Banerjee, S. Matsumoto, K. Mukaida, Y.-L.S. Tsai, WIMP dark matter in a well-tempered regime: a case study on singlet–doublets fermionic WIMP, arXiv:1603.07387.
[29] M. Kakizaki, A. Santa, O. Seto, Phenomenological signatures of mixed complex scalar WIMP dark matter, arXiv:1609.06555.

[30] ATLAS collaboration, G. Aad, et al., Observation of a new particle in the search for the Standard Model Higgs boson with the ATLAS detector at the LHC, Phys. Lett. B 716 (2012) 1–29, arXiv:1207.7214.
[31] CMS collaboration, S. Chatrchyan, et al., Observation of a new boson at a mass of 125 GeV with the CMS experiment at the LHC, Phys. Lett. B 716 (2012) 30–61, arXiv:1207.7235.
[32] Particle Data Group collaboration, K.A. Olive, et al., Review of particle physics, Chin. Phys. C 38 (2014) 090001.
[33] M. Ciuchini, E. Franco, S. Mishima, L. Silvestrini, Electroweak precision observables, new physics and the nature of a 126 GeV Higgs boson, J. High Energy Phys. 08 (2013) 106, arXiv:1306.4644.
[34] Gfitter Group collaboration, M. Baak, J. Cúth, J. Haller, A. Hoecker, R. Kogler, K. Mönig, et al., The global electroweak fit at NNLO and prospects for the LHC and ILC, Eur. Phys. J. C 74 (2014) 3046, arXiv:1407.3792.
[35] J. de Blas, M. Ciuchini, E. Franco, S. Mishima, M. Pierini, L. Reina, et al., Electroweak precision observables and Higgs-boson signal strengths in the Standard Model and beyond: present and future, arXiv:1608.01509.
[36] CEPC–SPPC Study Group collaboration, CEPC–SPPC Preliminary Conceptual Design Report. 1. Physics and Detector, IHEP-CEPC-DR-2015-01, IHEP-TH-2015-01, HEP-EP-2015-01.
[37] M. McCullough, An indirect model-dependent probe of the Higgs self-coupling, Phys. Rev. D 90 (2014) 015001, arXiv:1312.3322.
[38] C. Shen, S.-h. Zhu, Anomalous Higgs-top coupling pollution of the triple Higgs coupling extraction at a future high-luminosity electron–positron collider, Phys. Rev. D 92 (2015) 094001, arXiv:1504.05626.
[39] F.P. Huang, P.-H. Gu, P.-F. Yin, Z.-H. Yu, X. Zhang, Testing the electroweak phase transition and electroweak baryogenesis at the LHC and a circular electron–positron collider, Phys. Rev. D 93 (2016) 103515, arXiv:1511.03969.
[40] A. Kobakhidze, N. Liu, L. Wu, J. Yue, Implications of CP-violating top-Higgs couplings at LHC and Higgs factories, arXiv:1610.06676.
[41] J. Fan, M. Reece, L.-T. Wang, Precision natural SUSY at CEPC, FCC-ee, and ILC, J. High Energy Phys. 08 (2015) 152, arXiv:1412.3107.
[42] Q.-H. Cao, H.-R. Wang, Y. Zhang, Probing $HZ\gamma$ and $H\gamma\gamma$ anomalous couplings in the process $e^+e^- \to H\gamma$, Chin. Phys. C 39 (2015) 113102, arXiv:1505.00654.
[43] S.L. Hu, N. Liu, J. Ren, L. Wu, Revisiting associated production of 125 GeV Higgs boson with a photon at a Higgs factory, J. Phys. G 41 (2014) 125004, arXiv:1402.3050.
[44] S. Gori, J. Gu, L.-T. Wang, The $Zb\overline{b}$ couplings at future e^+e^- colliders, J. High Energy Phys. 04 (2016) 062, arXiv:1508.07010.
[45] K. Harigaya, K. Ichikawa, A. Kundu, S. Matsumoto, S. Shirai, Indirect probe of electroweak-interacting particles at future lepton colliders, J. High Energy Phys. 09 (2015) 105, arXiv:1504.03402.
[46] Q.-H. Cao, Y. Li, B. Yan, Y. Zhang, Z. Zhang, Probing dark particles indirectly at the CEPC, Nucl. Phys. B 909 (2016) 197–217, arXiv:1604.07536.
[47] S.-F. Ge, H.-J. He, R.-Q. Xiao, Probing new physics scales from Higgs and electroweak observables at e^+e^- Higgs factory, J. High Energy Phys. 10 (2016) 007, arXiv:1603.03385.
[48] M.E. Peskin, T. Takeuchi, A new constraint on a strongly interacting Higgs sector, Phys. Rev. Lett. 65 (1990) 964–967.
[49] M.E. Peskin, T. Takeuchi, Estimation of oblique electroweak corrections, Phys. Rev. D 46 (1992) 381–409.
[50] J. Fan, M. Reece, L.-T. Wang, Possible futures of electroweak precision: ILC, FCC-ee, and CEPC, J. High Energy Phys. 09 (2015) 196, arXiv:1411.1054.
[51] G. Altarelli, R. Barbieri, Vacuum polarization effects of new physics on electroweak processes, Phys. Lett. B 253 (1991) 161–167.
[52] G. Altarelli, R. Barbieri, S. Jadach, Toward a model independent analysis of electroweak data, Nucl. Phys. B 369 (1992) 3–32.
[53] H.-H. Zhang, Y. Cao, Q. Wang, The effects on S, T, and U from higher-dimensional fermion representations, Mod. Phys. Lett. A 22 (2007) 2533–2538, arXiv:hep-ph/0610094.
[54] H.-H. Zhang, W.-B. Yan, X.-S. Li, The oblique corrections from heavy scalars in irreducible representations, Mod. Phys. Lett. A 23 (2008) 637–646, arXiv:hep-ph/0612059.
[55] D.C. Kennedy, B.W. Lynn, Electroweak radiative corrections with an effective Lagrangian: four fermion processes, Nucl. Phys. B 322 (1989) 1–54.
[56] Z. Han, Effective theories and electroweak precision constraints, Int. J. Mod. Phys. A 23 (2008) 2653–2685, arXiv:0807.0490.
[57] P. Sikivie, L. Susskind, M.B. Voloshin, V.I. Zakharov, Isospin breaking in Technicolor models, Nucl. Phys. B 173 (1980) 189–207.
[58] H.-H. Zhang, A nondiagrammatic calculation of the rho parameter from heavy fermions, Eur. Phys. J. C 67 (2010) 51–56, arXiv:0911.4184.

[59] M. Awramik, M. Czakon, A. Freitas, G. Weiglein, Precise prediction for the W boson mass in the standard model, Phys. Rev. D 69 (2004) 053006, arXiv:hep-ph/0311148.
[60] M. Awramik, M. Czakon, A. Freitas, Electroweak two-loop corrections to the effective weak mixing angle, J. High Energy Phys. 11 (2006) 048, arXiv:hep-ph/0608099.
[61] A. Freitas, Higher-order electroweak corrections to the partial widths and branching ratios of the Z boson, J. High Energy Phys. 04 (2014) 070, arXiv:1401.2447.
[62] G.P. Lepage, P.B. Mackenzie, M.E. Peskin, Expected precision of Higgs boson partial widths within the standard model, arXiv:1404.0319.
[63] S. Bodenstein, C.A. Dominguez, K. Schilcher, H. Spiesberger, Hadronic contribution to the QED running coupling $\alpha(M_Z^2)$, Phys. Rev. D 86 (2012) 093013, arXiv:1209.4802.
[64] F. Jegerlehner, Hadronic vacuum polarization effects in alpha(em) (M(Z)), in: Electroweak Precision Data and the Higgs Mass. Workshop Proceedings, Zeuthen, Germany, February 28–March 1, 2003, pp. 97–112, arXiv:hep-ph/0308117.
[65] SLD Electroweak Group, DELPHI, ALEPH, SLD, SLD Heavy Flavour Group, OPAL, LEP Electroweak Working Group, L3 collaboration, S. Schael, et al., Precision electroweak measurements on the Z resonance, Phys. Rep. 427 (2006) 257–454, arXiv:hep-ex/0509008.
[66] ATLAS, CDF, CMS, D0 collaboration, First combination of Tevatron and LHC measurements of the top-quark mass, arXiv:1403.4427.
[67] J. Erler, Status of precision extractions of α_s and heavy quark masses, AIP Conf. Proc. 1701 (2016) 020009, arXiv:1412.4435.
[68] CMS collaboration, C. collaboration, Projected improvement of the accuracy of top-quark mass measurements at the upgraded LHC, CMS-PAS-FTR-13-017.
[69] ATLAS, CMS collaboration, G. Aad, et al., Combined measurement of the Higgs boson mass in pp collisions at $\sqrt{s} = 7$ and 8 TeV with the ATLAS and CMS experiments, Phys. Rev. Lett. 114 (2015) 191803, arXiv:1503.07589.
[70] A. Freitas, K. Hagiwara, S. Heinemeyer, P. Langacker, K. Moenig, M. Tanabashi, et al., Exploring quantum physics at the ILC, in: Proceedings, Community Summer Study 2013: Snowmass on the Mississippi, CSS2013, Minneapolis, MN, USA, July 29–August 6, 2013, arXiv:1307.3962.
[71] S. Mishima, Sensitivity to new physics from TLEP precision measurements, in: 6th TLEP Workshop, CERN, Geneva, Switzerland, October 16, 2013.
[72] H. Baer, T. Barklow, K. Fujii, Y. Gao, A. Hoang, S. Kanemura, et al., The International Linear Collider Technical Design Report – Volume 2: Physics, arXiv:1306.6352.
[73] A. Hocker, H. Lacker, S. Laplace, F. Le Diberder, A new approach to a global fit of the CKM matrix, Eur. Phys. J. C 21 (2001) 225–259, arXiv:hep-ph/0104062.
[74] H. Flacher, M. Goebel, J. Haller, A. Hocker, K. Monig, J. Stelzer, Revisiting the global electroweak fit of the standard model and beyond with Gfitter, Eur. Phys. J. C 60 (2009) 543–583, arXiv:0811.0009.
[75] R. Lafaye, T. Plehn, M. Rauch, D. Zerwas, M. Duhrssen, Measuring the Higgs sector, J. High Energy Phys. 08 (2009) 009, arXiv:0904.3866.
[76] F. Feroz, M.P. Hobson, E. Cameron, A.N. Pettitt, Importance nested sampling and the MultiNest algorithm, arXiv:1306.2144.
[77] J. Erler, P. Langacker, Implications of high precision experiments and the CDF top quark candidates, Phys. Rev. D 52 (1995) 441–450, arXiv:hep-ph/9411203.
[78] G. Passarino, M.J.G. Veltman, One loop corrections for e+ e− annihilation into mu+ mu− in the Weinberg model, Nucl. Phys. B 160 (1979) 151–207.
[79] A. Denner, Techniques for calculation of electroweak radiative corrections at the one loop level and results for W physics at LEP-200, Fortschr. Phys. 41 (1993) 307–420, arXiv:0709.1075.
[80] T. Hahn, M. Perez-Victoria, Automatized one loop calculations in four-dimensions and D-dimensions, Comput. Phys. Commun. 118 (1999) 153–165, arXiv:hep-ph/9807565.
[81] PandaX-II collaboration, A. Tan, et al., Dark matter results from first 98.7-day data of PandaX-II experiment, Phys. Rev. Lett. 117 (2016) 121303, arXiv:1607.07400.
[82] LUX collaboration, D.S. Akerib, et al., Results from a search for dark matter in the complete LUX exposure, arXiv:1608.07648.
[83] LUX collaboration, D.S. Akerib, et al., Results on the spin-dependent scattering of weakly interacting massive particles on nucleons from the Run 3 data of the LUX experiment, Phys. Rev. Lett. 116 (2016) 161302, arXiv:1602.03489.
[84] PICO collaboration, C. Amole, et al., Dark matter search results from the PICO-60 C_3F_8 bubble chamber, arXiv:1702.07666.

[85] J.R. Ellis, A. Ferstl, K.A. Olive, Reevaluation of the elastic scattering of supersymmetric dark matter, Phys. Lett. B 481 (2000) 304–314, arXiv:hep-ph/0001005.
[86] J.-M. Zheng, Z.-H. Yu, J.-W. Shao, X.-J. Bi, Z. Li, H.-H. Zhang, Constraining the interaction strength between dark matter and visible matter: I. Fermionic dark matter, Nucl. Phys. B 854 (2012) 350–374, arXiv:1012.2022.
[87] HERMES collaboration, A. Airapetian, et al., Precise determination of the spin structure function g(1) of the proton, deuteron and neutron, Phys. Rev. D 75 (2007) 012007, arXiv:hep-ex/0609039.